



HAL
open science

Migraine-Associated TRESK Mutations Increase Neuronal Excitability through Alternative Translation Initiation and Inhibition of TREK

Perrine Royal, Alba Andres-Bilbe, Pablo Ávalos Prado, Clément Verkest, Brigitte Wdziekonski, Sébastien Schaub, Anne Baron, Florian Lesage, Xavier Gasull, Joshua Levitz, et al.

► To cite this version:

Perrine Royal, Alba Andres-Bilbe, Pablo Ávalos Prado, Clément Verkest, Brigitte Wdziekonski, et al.. Migraine-Associated TRESK Mutations Increase Neuronal Excitability through Alternative Translation Initiation and Inhibition of TREK. *Neuron*, 2019, 101 (2), pp.232-245.e6. 10.1016/j.neuron.2018.11.039 . hal-02267115

HAL Id: hal-02267115

<https://hal.science/hal-02267115>

Submitted on 18 Aug 2019

HAL is a multi-disciplinary open access archive for the deposit and dissemination of scientific research documents, whether they are published or not. The documents may come from teaching and research institutions in France or abroad, or from public or private research centers.

L'archive ouverte pluridisciplinaire **HAL**, est destinée au dépôt et à la diffusion de documents scientifiques de niveau recherche, publiés ou non, émanant des établissements d'enseignement et de recherche français ou étrangers, des laboratoires publics ou privés.

Migraine-associated TRESK mutations increase neuronal excitability through alternative translation initiation and inhibition of TREK

Authors:

Perrine Royal^{1,2}, Alba Andres-Bilbe³, Pablo Ávalos Prado^{1,2}, Clément Verkest^{2,4}, Brigitte Wdziekonski^{1,2}, Sébastien Schaub¹, Anne Baron^{2,3}, Florian Lesage^{2,4}, Xavier Gasull³, Joshua Levitz⁵, Guillaume Sandoz^{1,2*}

Affiliations:

¹Université Cote d'Azur, CNRS, INSERM, iBV, France.

²Laboratories of Excellence, Ion Channel Science and Therapeutics Nice, France.

³Neurophysiology Laboratory, Department of Biomedicine, Medical School, Institute of Neurosciences, Universitat de Barcelona, IDIBAPS, Barcelona, Spain.

⁴Université Cote d'Azur, CNRS, INSERM, Institut de Pharmacologie Moléculaire et Cellulaire, France

⁵Department of Biochemistry, Weill Cornell Medicine, New York, NY.

*Correspondence to: sandoz@unice.fr

In brief: Royal et al. demonstrate that migraine-associated frameshift mutations of TRESK, a two-pore-domain K⁺ channel, lead to the production of a second protein fragment, which carries the pathophysiological function by inhibiting TREK1 and 2, due to a mechanism called frameshift mutation-induced Alternative Translation Initiation (fsATI).

Abstract:

Mutations in ion channels contribute to neurological disorders, but determining the basis of their role in pathophysiology is often unclear. In humans, 2 mutations have been found to produce a dominant negative for TRESK, a two-pore-domain K⁺ channel implicated in migraine: TRESK-MT, a 2 bp frameshift mutation (F139WfsX24) and TRESK-C110R, a missense mutation. Despite the fact that both mutants strongly inhibit TRESK, only TRESK-MT leads to an increase in sensory neuron excitability and is associated with a migraine phenotype. Here, we identify a new mechanism, termed frameshift mutation induced Alternative Translation Initiation (fsATI) that explains why TRESK-MT but not TRESK-C110R is associated with migraine disorder. fsATI leads, from the same TRESK-MT mRNA, to two proteins: TRESK-MT1 and TRESK-MT2. We show that by co-assembling with and inhibiting TREK1 and TREK2, another subfamily of K_{2P} channels, TRESK-MT2 increases trigeminal sensory neuron excitability, a key component of migraine induction, leading to a migraine-like phenotype. This finding identifies TREK as a molecular target in migraine pathophysiology and resolves the contradictory lack of effect of TRESK-C110R which targets only TRESK and not TREK. Finally, taking into account the potential for fsATI allowed us to identify a new migraine-related TRESK mutant, Y121LfsX44, which also leads to the production of two TRESK fragments, indicating that this mechanism may be widespread. Together, our results suggest that genetic analysis of disease-related mutations should consider fsATI as a distinct class of mutations.

Key Words: K_{2P} channels, leak current, migraine, alternative translation initiation, frameshift mutation, neuronal excitability, sensory neuron, single molecule fluorescence, pain, KCNK

Introduction

Migraine is a common, disabling neurological disorder with a genetic, environmental and hormonal component with an annual prevalence estimated at ~15%. It is characterized by attacks of severe, usually unilateral and throbbing headache, and can be accompanied by nausea, vomiting and photophobia. Migraine is clinically divided into two main subtypes, migraine with aura (MA) when a migraine is preceded by transient neurological disturbances which are usually visual and migraine without aura (MO). Cortical spreading depression (CSD) underlies the aura, although its precise relationship to headache is unclear. Activation and sensitization of trigeminal neurons (TG) leading to the release of pro-inflammatory peptides is likely a key component in pain initiation and transmission in migraine (Nosedá and Burstein, 2013) (Yan and Dussor, 2014).

Recent evidence points to a pivotal contribution of a variety of two-pore domain potassium (K_{2P}) channels in chronic pain processing. The diverse K_{2P} channel family is made of 15 subtypes which form 6 subfamilies. The activity of these channels drives the membrane potential toward the K⁺ equilibrium potential and therefore reduces cellular excitability. Expression of several K_{2P} channel subunits has been detected in nociceptive dorsal root ganglion and trigeminal neurons (Alloui et al., 2006; Bautista et al., 2008; Blin et al., 2016; Morenilla-Palao et al., 2014; Noël et al., 2009; Yamamoto et al., 2009). One subtype of K_{2P} channels that is highly expressed in sensory neurons, TRESK, has been directly linked to MA via a causally linked 2 bp frameshift mutation (F139WfsX24) identified in the *KCNK18* gene which causes premature truncation of TRESK (“TRESK-MT”) (Lafrenière et al., 2010; Wood, 2010). This mutation segregated perfectly with the MA phenotype in a large pedigree and was shown to produce a non-functional protein that can serve as a dominant-negative that functionally downregulates the wild type (WT) TRESK channel (Lafrenière et al., 2010; Wood, 2010). TRESK-MT has been shown to induce hyperexcitability of TG neurons (Guo et al., 2014; Liu et al., 2013), which likely underscores its role in migraine. However, in subsequent genetic screening studies, another missense TRESK variant, C110R, was identified (Andres-Enguix et al., 2012). TRESK-C110R, similar to TRESK-MT, exerts a dominant

negative effect on WT-TRESK in heterologous cells, but expression of this mutant was found to have no effect on TG excitability (Guo et al., 2014). This absence of effect explains why this mutant was found in both migraine patients and control subjects (Guo et al., 2014). Therefore, despite the fact that both mutations lead to the same apparent effect on TRESK function, only TRESK-MT is able to increase TG excitability and is linked to migraine pathophysiology.

Classically a eukaryotic mRNA is thought to contain one translation start codon which allows the production of a single protein species. However, in some cases, eukaryotic ribosomes can recognize several alternative translation start sites to induce the formation of several different proteins from the same mRNA (Kochetov, 2008). This alternative translation initiation is a means of expanding the proteome (Kochetov, 2008) and has been shown to increase the functional diversity of K_{2P} channels (Thomas et al., 2008), raising the possibility that it plays a role in TRESK-mediated migraine pathophysiology.

In this study, we addressed why TRESK-MT (F139WfsX24), but not TRESK-C110R, is able to increase TG excitability and, potentially, play a role in migraines. Using single molecule fluorescence and chemical optogenetic methods, we found that TRESK is able to heterodimerize with 2 distantly-related K_{2P} channels from another subfamily, TREK1 and TREK2 and that TRESK-MT strongly inhibits TRESK, TREK1, and TREK2 currents. In stark contrast, we show that TRESK-C110R is only able to inhibit TRESK, but not TREK1 or TREK2. Furthermore, we show, using double KO mice for TREK1 and TREK2, that TRESK-MT increases TG neuronal excitability by inhibiting TREK1 and TREK2. Consistent with a role for TREK1 and TREK2 in migraine induction, we found that double KO mice for TREK1 and TREK2 present, at rest, a migraine-like allodynia phenotype. These results resolve the contradictory lack of effect of TRESK-C110R which targets only TRESK and not TREK1 or TREK2. Strikingly, we next find that the 2 bp frameshift mutation of TRESK-MT puts an alternative start codon in frame which leads to the translation of a second TRESK fragment, termed MT2, which specifically co-assembles with TREK1 and TREK2 to downregulate their function leading to the TG excitability increase. Consistent with a role for

MT2 in migraine induction, we found that MT2 expression within the trigeminal ganglia induced a migraine-like allodynia phenotype in rat. Finally, we find that other previously uncharacterized migraine-associated TRESK mutations also produce multiple fragments via alternative translation initiation (ATI) that can have distinct effects on TRESK and TREK channels. Together these findings identify frameshift induced-alternative translation initiation (fsATI) as a mechanism initiated by TRESK mutations which leads to two protein fragments with dominant negative effects on distinct channel targets to, ultimately, increase sensory neuron excitability which may contribute to migraine induction.

Results

TRESK heteromerizes with TREK1 and TREK2

Despite the fact that K_{2P} channels share a similar architecture and global function, they share a low level of sequence identity, even between members of the same subfamily. Surprisingly, this low level of identity does not preclude heteromerization, as we and others recently showed within the TREK subfamily (Blin et al., 2016; Hwang et al., 2014; Lengyel et al., 2016; Levitz et al., 2016). Based on this and the fact that TG neurons express many K_{2P} channels (TREK1, TREK2, TRAAK, TASK1 and TASK3) (Bautista et al., 2008; Yamamoto et al., 2009), we hypothesized that the difference between TRESK mutants is due to their differential ability to modify the function of other K_{2P} channels through heteromerization. To assess the ability of TRESK to heteromerize with other K_{2P} channels which are expressed in TG neurons, we used the single-molecule pull-down (“SiMPull”) assay (Jain et al., 2012) to visualize individual antibody-immobilized protein complexes on polyethylene glycol-passivated glass coverslips (Figure 1A). We co-expressed GFP-TRESK with either HA-TRESK, HA-TREK1, HA-TREK2, HA-TRAAK, HA-TASK1, or HA-TASK3 and assessed their ability to co-immunoprecipitate (Co-IP) GFP-TRESK *via* an anti-HA antibody. HA-TRESK, HA-TREK1, and HA-TREK2, were able to co-IP many fluorescent GFP-TRESK spots (Figure 1B, C), whereas no GFP-TRESK spots were observed for HA-TRAAK, HA-TASK1 or HA-TASK3 (Figure 1C), indicating that TRESK co-assembly with other K_{2P} channels is specific for TREK1 and TREK2. Importantly, controls showed that identical results were observed in two different non-ionic detergents (Figure 1C), that similar expression levels were seen for GFP-TRESK when co-expressed with HA-TREK1 or HA-TRESK (Figure S1A), that all HA-tagged K_{2P} constructs were able to pull down themselves (Figure S1B, C), that pulldown was dependent on the presence of the anti-HA antibody (Figure S1D) and confirm that TREK1, TREK2 and TRESK are coexpressed in the same cultured trigeminal (TG) neurons using immunofluorescence and single cell RT-PCR (Figure S1F).

We next used photobleaching step analysis (Ulbrich and Isacoff, 2007) to determine the stoichiometry of TREK1 and TRESK complexes to test the hypothesis that they form heterodimers. First we confirmed that HA-GFP-TREK1 form homodimers in our assay by observing ~70% 2-step bleaching

for each when expressed and immunoprecipitated alone with anti-HA antibodies (Figure S2A), consistent with the formation of strict dimers with a GFP maturation rate of ~80%. Then, we counted the number of GFP-TRESK subunits within a HA-TREK1/GFP-TRESK complex by observing bleaching steps of GFP-TRESK co-immunoprecipitated with immobilized HA-TREK1 (Figure S2C). The majority of fluorescence intensity trajectories showed one bleaching step (~70%) (Figure S2C). This distribution is similar to the one observed for HA-TREK1/GFP-TREK1 complexes (Figure S2B) and agrees well with a 1:1 stoichiometry showing that TREK1-TRESK is primarily a heterodimer.

To test the functionality of the TREK1-TRESK heterodimer, we developed a heterodimerization assay based on an engineered “Photoswitchable Conditional Subunit” (TREK1-PCS) of TREK1. The TREK1-PCS is a TREK1 subunit where the C-terminus has been deleted to produce endoplasmic reticulum retention, which can be rescued through co-assembly with a full-length subunit (Sandoz et al., 2012). Following co-assembly and surface targeting, TREK1-PCS can then optically control the channel via a tethered photoswitchable blocker (“MAQ”) which attaches to a genetically engineered cysteine. Therefore, gain of photosensitivity of an identified co-expressed TREK interacting subunit allows for the verification of a functional heteromer with TREK1. As expected, expression of TREK1-PCS alone did not generate a photoswitchable current (Figure 1D) but co-expression with either TREK1 or TRESK induced a robust photoswitchable current (Figure 1E, F), indicating that the TRESK subunit is able to co-assemble with TREK1-PCS. Consistent with SiMPull data, no photocurrent was observed when TASK1 (Figure 1G) or TASK3 (Figure S1E) were co-expressed with TREK1-PCS. Furthermore, the bleaching step distribution of GFP-TREK1-PCS spots co-immunoprecipitated with immobilized HA-TREK1 is similar to HA-TREK1/GFP-TREK1, the majority of fluorescence spots showed one bleaching step (~70%) (Figure S2D), supporting the conclusion that the light-gated TREK1-PCS/TRESK current is carried by a TREK1-PCS/TRESK heterodimer with a common pore.

Next, to test the functional properties of the TREK1-TRESK heteromer, we constructed a linked, tandem dimer to have a uniform representation at the surface of the cell of the TREK1-TRESK heteromer (Figure S3). This heteromeric channel displayed properties which are a mix of those from TREK1 and

TRESK homodimers. Notably, TRESK is insensitive to arachidonic acid while TREK1 is sensitive (Figure S3A, B, C) and TRESK-TREK1 tandems show an intermediate sensitivity to arachidonic acid (Figure S3C). Furthermore, similar to TRESK, but not TREK1, TRESK-TREK1 tandems showed sensitivity to intracellular calcium, as tested with ionomycin application (Figure S3D, F). Consistent with this, the light-gated TREK1-PCS/TRESK current is also calcium sensitive (Figure S3E, F), confirming that the light-gated TREK1-PCS/TRESK current is carried by a TRESK1-TRESK heteromer with a common pore.

Having found that TREK can physically and functionally heteromerize with TRESK and that all three channel subtypes are co-expressed in sensory neurons, we next investigated the ability of TRESK mutants to modify TREK1 and TREK2 currents.

TRESK-MT, but not TRESK-C110R, acts as a dominant negative on TREK1 and TREK2 channels

As previously shown (Andres-Enguix et al., 2012), both TRESK-MT and TRESK-C110R exert a dominant-negative effect on whole cell TRESK currents (Figure 2A-C). Since TREK1 can co-assemble with TRESK (Figure 1), we addressed the impact of the MT and C110R variants on TREK1 current. We found that TRESK-C110R co-expression did not modify TREK1 current whereas TRESK-MT co-expression induced a near-complete inhibition of TREK1 current (Figure 2D-F). Similar to TREK1, TRESK-MT, but not TRESK-C110R strongly inhibited, TREK2 current (Figure 2G-I). This dominant negative effect is specific and likely dependent on co-assembly since TASK1, TASK3 and TRAAK, which do not co-IP with TRESK (Figure 1), were not sensitive to TRESK-MT co-expression (Figure S4). To address why TRESK-C110R does not modify TREK1 or TREK2 current, we used the SiMPull assay to test the ability of TRESK-C110R to physically interact with TREK1. We co-expressed HA-TREK1 with either GFP-TRESK or GFP-TRESK-C110R and tested their ability to be co-immunoprecipitated (Co-IP) with HA-TREK1 *via* an anti-HA antibody. Whereas GFP-TRESK was able to be co-immunoprecipitated with HA-TREK1 leading to many fluorescent spots, very few spots were observed for GFP-TRESK-C110R (Figure S5A). This indicates that TREK1 can co-assemble with TRESK and that the C110R mutation leads

to a drastic reduction of this association explaining why TRESK-C110R have no effect on TREK1 current. Together these data show that TRESK-MT can inhibit TRESK, TREK1 and TREK2 whereas TRESK-C110R is only able to inhibit TRESK. Based on the fact that TRESK-MT but not TRESK-C110R is able to induce TG neuron hyperexcitability (Guo et al., 2014; Liu et al., 2013), we hypothesized that TRESK-MT induces sensory neuron hyper-excitability primarily by acting on TREK1 and TREK2, not TRESK.

TRESK-MT increases neuronal excitability through the inhibition of TREK1 and TREK2

To investigate the role of TREK1 and TREK2 in the induction of TG hyperexcitability by TRESK-MT, we tested if overexpression of GFP-TRESK-MT alters the passive and active electrophysiological properties of small-diameter (<25 μm) TG neurons from wild-type or TREK1/TREK2 double knockout (TREK1^{-/-}/TREK2^{-/-}) mice. As previously shown, TRESK-MT expression in WT TG neurons led to a decrease of the lamotrigine current (Figure S6) leading to an increase in excitability (Figure 3C) which included a decrease in the rheobase (74 ± 11 pA vs 47 ± 5 pA, $P < 0.05$ for TG neurons expressing GFP or TRESK-MT, respectively) and an increase in the number of action potentials (APs) evoked by suprathreshold current injections compared to control (Figure 3A, C). As shown in Figure 3B, neurons from TREK1^{-/-}/TREK2^{-/-} mice were more excitable than WT TG neurons. These neurons have a smaller lamotrigine current (Figure S6), smaller rheobase (55 ± 6 pA, $P < 0.05$) and a significant increase in the number of APs evoked by suprathreshold current injections compare to WT TG neurons. Consistent with a role for TREK1 and 2 in mediating the effects of TRESK-MT, TRESK-MT overexpression did not alter the excitability of TREK1^{-/-}/TREK2^{-/-} mice (Figure 3D). TREK1^{-/-}/TREK2^{-/-} TG neurons showed no increase in the number of evoked APs number nor a reduction in rheobase (55 ± 6 pA vs 53 ± 5 pA, for TG neuron expressing GFP or TRESK-MT respectively, $P > 0.5$). Together these data strongly support a major role for TREK1 and TREK2 in the control of TG neuron excitability and support the idea that TRESK-MT differs functionally from TRESK-C110R in its ability to target TREK1 and TREK2 to increase the excitability of TG neurons which is likely a crucial step in the induction of migraines.

TREK1^{-/-}/TREK2^{-/-} mice show a mechanical allodynia which is not increased by NO donors

Having found that expression of the TREK-MT mutant increases TG excitability through TREK1-TREK2 inhibition, we hypothesized that TREK1^{-/-}/TREK2^{-/-} mice would show an increased susceptibility to a migraine-related phenotype. Migraine is associated with an increase of the sensitivity to all sensory modalities and cutaneous allodynia can be used as a quantifiable marker of migraine disorder (Bates et al., 2010; Pradhan et al., 2014; Verkest et al., 2018). One approach to model acute and chronic migraine is the quantification of this increase in response to known migraine triggers such as nitric oxide (NO) donors (Bates et al., 2010), including isosorbide dinitrate (ISDN) (Verkest et al., 2018). We quantified ISDN-evoked mechanical hyperalgesia in TREK1^{-/-}/TREK2^{-/-} and wild-type controls in acute and chronic conditions. In a first experiment, paw mechanical nociception thresholds were determined with a dynamic von Frey aesthesiometer before and during a 3-hour period after intraperitoneal injection of ISDN (10 mg/kg) (Figure 3E) (Bates et al., 2010; Verkest et al., 2018). In a second experiment, we assessed mechanical nociception thresholds in both TREK1^{-/-}/TREK2^{-/-} and wild-type controls, by intraperitoneally injecting ISDN every day for four days as a model of chronic migraine-associated pain (Figure 3E). We found that, at rest, TREK1^{-/-}/TREK2^{-/-} mice showed a decreased mechanical threshold compared to WT mice (2.6 ± 0.1 g vs 3.9 ± 0.1 g; $P < 0.001$). Notably, the basal mechanical threshold of TREK1^{-/-}/TREK2^{-/-} mice is similar to the threshold observed 1.5 hours after acute ISDN injection in WT mice (Figure 3F, $P = 0.831$). In the acute model experiment, during the first 1.5 hours following ISDN injection, the mechanical thresholds remained significantly lower in TREK1^{-/-}/TREK2^{-/-} mice than in wild-type controls (Figure 3F, $P < 0.001$ after 30 minutes and $P < 0.01$ after 1 hour with a linear mixed-effects model). In the chronic migraine-associated pain assay, the mechanical thresholds remained significantly lower for TREK1^{-/-}/TREK2^{-/-} mice compared to wild-type controls but the difference was strongly reduced (Δ mechanical threshold 0.33 ± 0.2 g vs 1.12 ± 0.1 g) (Figure 3G).

Having found that ISDN did not change the mechanical threshold in both acute and chronic migraine-associated pain models in TREK1^{-/-}/TREK2^{-/-} mice, we wondered if a treatment used in prophylaxis in migraine patient, topiramate, could reverse this observed migraine-like phenotype as was

observed for both models of NO donor-induced migraine (Pradhan et al., 2014). We assessed the mechanical nociception threshold in TREK1^{-/-}/TREK2^{-/-} mice before and 2 hours following the intraperitoneal injection of 30 mg/kg of topiramate. Treatment with topiramate reversed the chronic basal hyperalgesia seen in TREK1^{-/-}/TREK2^{-/-} mice (1.2 ± 0.2 g; Figure 3H), as was previously observed for a nitroglycerin-evoked form of hyperalgesia (Pradhan et al., 2014). As a control, we tested non-treated ISDN WT mice and did not observe any significant shift of the mechanical threshold following topiramate treatment (Figure 3H).

These data demonstrate that at rest the TREK1^{-/-}/TREK2^{-/-} mice present a hyperalgesia phenotype which is similar to the phenotype observed in ISDN-treated animals. This is consistent with a role of TREK1/TREK2 in sensory neuron hypersensitivity that is relevant to migraine and this phenotype is partially reversed by topiramate, a drug used in the clinic to treat chronic migraine.

TRESK-MT mutation induces the translation of a second protein, MT2

We next explored how TRESK-MT exerts its effects on TREK channels at the molecular level. The F139WfsX24 frameshift mutation of TRESK-MT results in the premature truncation of the human TRESK protein from 384 amino acids (aa) to 162 aa. The truncated TRESK includes the first 138 aa of wild-type TRESK followed by a 24 aa aberrant sequence. The corresponding mutation has very similar effects on the mouse TRESK gene, generating a truncated protein with the first 149 aa of wild-type TRESK and followed by a 50 aa aberrant sequence at the C terminus (Figure 4B). We fused a GFP tag to the N-terminus of the mouse TRESK-MT and tested its ability to be immobilized by HA-TRESK, HA-TREK1 or HA-TREK2 in the SiMPull assay. Surprisingly, only HA-TRESK was able to co-IP GFP-TRESK-MT via an anti-HA antibody (Figure 4A). This result confirms that TRESK-MT associates with TRESK to induce its dominant negative effect but raises the question of how TRESK-MT is able to inhibit TREK1 and TREK2 without direct association.

It has been hypothesized that alternative translation initiation (ATI) of eukaryotic mRNAs, including those that encode K_{2P} channels (Thomas et al., 2008), may provide a method to expand the

proteome (Kochetov, 2008). A close examination of the nucleotide sequence of TRESK-MT revealed that the F139WfsX24 frameshift mutation places two new ATG codons in frame with the reference open reading frame of TRESK (ATGs at position +356 and +407 for the human TRESK cDNA and +389 and +490 for the mouse cDNA). We hypothesized that one of these codons may serve as an ATI site that can lead to the formation of a second truncated TRESK protein, termed “MT2”, that would include a short (either 2 or 19 aa) N-terminal aberrant sequence followed by the C-terminal part of TM2, including the 2-3 intracellular loop, TM3, P2 loop, TM4 and the C terminal domains (Figure 4B). To test whether MT2 is co-translated with MT1, we introduced an N-terminal mCherry-tag in frame with MT1 and a C-terminal GFP in frame with MT2 within the mouse TRESK-MT cDNA (“mCherry-TRESK-MT-GFP”). Expression of this construct led to HEK 293T cells with both mCherry and GFP fluorescence, showing the co-translation of mCherry-MT1 and MT2-GFP (Figure 4C). This co-translation was observed in other cell lines including MDCK cells (Figure 4C), as well as in primary TG neurons (Figure 4C). Next, we introduced an N-terminal hemagglutinin (HA) tag in frame with MT1 and another one in frame with MT2 within the mouse TRESK-MT cDNA (“HA-TRESK-MT-HA”). Lysate from cells transfected with HA-TRESK-MT-HA was probed in a western blot with anti-HA antibodies and 2 bands, with a similar intensity, corresponding to the expected molecular weights for MT1 (~23 kDa) and MT2 (~29 kDa) were detected (Figure 4D). Together these data clearly show that TRESK-MT leads to the production of two distinct fragments of TRESK.

To probe the function of MT2, we introduced a stop codon into the MT2 ORF of TRESK-MT at the beginning of the 2-3 loop (Figure 4B) inducing the loss of expression of MT2 (Figure S7A). As shown in Figure 5, whereas the introduction of the stop codon in the MT2 ORF did not change the ability of TRESK-MT to inhibit TRESK current (Figure 5B), this stop codon abolished the ability of TRESK-MT to produce a dominant negative functional effect on TREK1 (Figure 5A). We next confirmed the importance of this second ORF by mutating, in TRESK-MT, the putative ATI start codons one by one. Mutation of the first ATG abolished the ability of TRESK-MT to inhibit TREK1 (Figure 5C), but not TRESK (Figure 5D) whereas mutation of the second ATG did not alter the ability of TRESK-MT to inhibit TREK1 current (Figure 5C and Figure S7B). This data indicates that the ATI site is the first internal ATG. As a control, we

mutated a third ATG, which is also present in the WT-TRESK sequence, and found that it did not change the ability of TRESK-MT to inhibit both TRESK and TREK1 currents (Figure 5C and Figure S7C). Similar to TREK1, introduction of a stop codon into the MT2 ORF or mutation of the first ATG also abolished the inhibition of TREK2 by TRESK-MT (Figure 5E, F). To further demonstrate that the first ATG serves as a start codon, we mutated the potential Kozak sequence **GCTATGG** to **CCTATGC** and found that alteration of the Kozak sequence strongly reduced the inhibitory effect of TRESK-MT on TREK1 current (Figure 5C and Figure S7D) without affecting the effect on TRESK (Figure 5D and Figure S7E).

MT2, but not MT1, by acting as a dominant negative on TREK1 and TREK2 channels, increases neuronal excitability of WT small TG neurons leading to facial allodynia

To independently express MT1 and MT2 for functional characterization, we sub-cloned both ORFs into separate mammalian expression vectors. Co-expression of MT2 with TRESK did not modify TRESK current (Figure 6B, E), while MT1 co-expression induced a ~3-fold decrease of the current which was similar to what was observed for the co-expression of the full TRESK-MT construct (Figure 6A, E). On the contrary, co-expression of MT1 did not modify TREK1 current (Figure 6C, E) but co-expression of MT2 induced a ~4-fold decrease of the current, similar to what was observed with co-expression of the full TRESK-MT construct (Figure 6D, E). Similar results were obtained for TREK2 (Figure 6E, Figure S8). Consistent with the functional data, we found that GFP-MT2 is co-immunoprecipitated with HA-TREK1 or HA-TREK2 in the SiMPull assay (Figure 6F).

To validate the physiological role of interaction between TREK1, TREK2 and MT2, we tested the functional effect of MT2 in TG neurons. Whereas MT1 expression did not alter the excitability of WT TG neurons (Figure 7A, B), MT2 increased it significantly (Figure 7A, C). In fact, MT1 did not modify the rheobase (74 ± 11 pA vs 79 ± 5 pA, $P > 0.5$ for TG neurons expressing GFP or MT1, respectively) and did not modify the number of action potentials (APs) evoked by suprathreshold current injections compared to control. Conversely, MT2 expression in WT TG neurons led to an increase in excitability (Figure 7) which included a decrease in the rheobase (74 ± 11 pA vs 55 ± 5 pA, $P < 0.05$ for TG neurons expressing GFP or

MT2, respectively, $P < 0.05$) and an increase in the number of action potentials (APs) evoked by suprathreshold current injections compared to control (Figure 7A, C). We confirmed that this effect is linked to TREK1 and TREK2 since MT2 overexpression failed to increase the excitability of TREK1^{-/-}/TREK2^{-/-} TG neurons (Figure 7D).

Having found that MT2, by inhibiting TREK1 and TREK2, is sufficient to increase TG excitability we asked if MT2 expression in TG ganglia would induce a migraine-related phenotype. We conducted behavioral experiments in rats in which MT2 was virally overexpressed within the trigeminal ganglia. Rats allow to test the mechanical pain threshold on the face which is directly linked to TG excitability, constituting a relatively direct, reliable and quantifiable marker of migraine disorder in clinical contexts as well as in NO-induced migraine (Pradhan et al., 2014; Kopruszinski et al., 2017; Harris et al., 2017). As shown in Figure 7F, MT2 expression in TG ganglia (Figure S9) significantly increased the facial mechanical threshold (3.3 ± 0.4 g vs 7.7 ± 0.4 g, $P < 0.001$). Furthermore, as was seen for the TREK1^{-/-}/TREK2^{-/-} mice, the basal mechanical facial threshold of MT2-expressing rats is similar to the threshold observed 1.5, 2 and 3 hours after acute ISDN injection in WT rats. Having found that MT2 overexpression induced allodynia, we quantified ISDN-evoked mechanical hyperalgesia and found that MT2 overexpression prevents the effect of ISDN, similarly to what was observed for TREK1^{-/-}/TREK2^{-/-} mice.

Together these data demonstrate that at rest MT2 leads to an increase in TG excitability and a chronic cutaneous allodynia similar to the one observed following NO-donor injection and in TREK1^{-/-}/TREK2^{-/-} double KO mice.

MT2-producing alternative translation initiation is found in other migraine-associated TRESK mutants

Having found that MT2 is responsible for the migraine-associated increase in TG excitability and induction of a migraine-like phenotype through the inhibition of TREK1 and TREK2, we anticipated that other frameshift mutations may exist which place the ATG at position +356 in-frame with the reference open reading frame of TRESK. Such mutations would lead to the formation of MT2. This mutation could

be either a 2 bp deletion or 1 bp insertion in the region between the ATG at position +356 and the TGA at position +427 (Figure S10). We used the Exome Aggregation Consortium (ExAC) database (Lek et al., 2016) and found one variant (Y121LfsX44) with a T duplication (+1 pb, c.361dupT) that places the ATG site in frame with the TRESK ORF (Figure S9). We introduced this insertion into the mCherry-TRESK-GFP (mCherry-TRESK-c.361dupT-GFP) sequence and found, similar to mCherry-TRESK-MT-GFP (Figure 4C), that this construct led to HEK 293T cells with both mCherry and GFP fluorescence (Figure 8A) due to the co-translation of both MT1 and MT2 proteins. Similar to TRESK-MT, this mutant is able to inhibit both TRESK, TREK1 and TREK2 (Figure 8). As was seen for TRESK-MT (Figure 5), introduction of a stop codon into the MT2 ORF (TRESK c.361dupT_{STOP}) of this mutant abolished its ability to inhibit TREK1 and TREK2 (Figure 8), but not TRESK. Since this Y121LfsX44 mutation leads to the same molecular effects as TRESK-MT on TREK function, we hypothesized that it may be associated with a migraine phenotype. To address this, we looked in the ClinVar database (Landrum et al., 2016) and found that this mutant has been correlated with a migraine phenotype (RCV000490385.1).

Discussion

While initial findings of migraine-associated mutations of TRESK represented a major breakthrough (Lafrenière et al., 2010), a direct relationship between TRESK channel disruption and migraine has been challenged based on the discovery of a TRESK mutation (C110R) which produces a dominant negative form of TRESK but is found in a control cohort population (Andres-Enguix et al., 2012). The presence of this mutation in control individuals indicates that a single non-functional TRESK variant alone may not be sufficient to cause migraines, consistent with the genetic complexity of this disorder. In this study, we have addressed this controversy and found that the migraine-associated mutation of TRESK exerts its effects on sensory neurons by associating and serving as a dominant negative not only for TRESK, but also for TREK1 and TREK2 channels. In stark contrast, TRESK-C110R is not able to regulate TREK channels. Consistent with a function of TREK1 and TREK2 in TRESK-MT-induced migraine, the TREK1^{-/-}/TREK2^{-/-} mice show a migraine-like hypersensitivity to mechanical stimuli. Surprisingly, we find that migraine-associated frameshift mutations of TRESK induce alternative translation initiation which allows the formation of a second product, MT2, which mediates the dominant negative action on TREK1 and TREK2. This dominant negative action on TREK1 and TREK2, ultimately, leads to an increase in TG neuron excitability and a migraine-like hypersensitivity to facial mechanical stimuli. Supporting this phenomenon as a general mechanism, we found another migraine-associated frameshift mutation in TRESK that produces a similar ORF shift which also leads to the formation of MT2. Together these findings support a role of frameshift induced alternative translation initiation (fsATI) and for TREK potassium channels as a key part of sensory neuron excitability and the underlying cellular mechanism of migraine.

We and others (Blin et al., 2016; Hwang et al., 2014; Lengyel et al., 2016; Levitz et al., 2016) have recently shown that K_{2P} channels are able to form both homodimeric and heterodimeric potassium channels. In this study, we show that TREK and TRESK readily assemble as heteromers. We show that this TRESK-TREK heteromer is a functional dimer since one TRESK is able to co-assemble with one TREK subunit to form a heterodimeric channel with a common pore using a photoswitchable conditional TREK1 (Sandoz et al., 2012). This is quite surprising given that TREK1/2 and TRESK are in different K_{2P} channel subfamilies

and only show low sequence identity of ~19.7% (Sano et al., 2003). We previously found that all members of the TREK channel subfamily (TREK1, TREK2, and TRAAK) can co-assemble but that TREK was unable to interact with TASK channels. Similar to the other reported heteromers, TREK1-TRESK heterodimers show unique biophysical behavior that blends the properties of the parent subunits. Notably, TREK1-TRESK is both arachidonic acid- and calcium-sensitive. In this study, we also show that TRESK does not heteromerize with three other K_{2P} channels, one from the TREK subfamily, TRAAK, and two from the TASK subfamily TASK1 and TASK3. Together this indicates that not all pairs of K_{2P} channel subunits are able to interact and that there are indeed rules of interaction that remain to be deciphered. Future work will be needed to determine the molecular mechanisms and structural interfaces that mediate specific K_{2P} heteromer assembly and the associated functional consequences of heteromerization.

TRESK channels are expressed in the dorsal root ganglion (DRG) and show their highest expression levels in trigeminal ganglion (TG). In DRG and TG, TRESK is most abundant in the small and medium-size sensory neurons (Dobler et al., 2007) (Lafrenière et al., 2010). In TG neurons, introduction of TRESK-MT has been shown to reduce the lamotrigine-sensitive K^+ current leading to an increase in excitability (Guo et al., 2014; Liu et al., 2013). This increase of TG excitability cannot be explained by TRESK inhibition since TRESK-C110R, which also strongly inhibits wild-type TRESK, does not inhibit the lamotrigine-sensitive K^+ current and does not increase TG excitability, explaining its lack of involvement in migraine (Guo et al., 2014). TREK1 and TREK2 are also expressed in DRG and show high expression levels in TG (Blin et al., 2016; Yamamoto et al., 2009). Furthermore, TREK1 and TREK2 have recently been shown to also be lamotrigine-sensitive (Walsh et al., 2016 and Figure S6A, B). We found that TRESK-MT inhibits TREK1 and TREK2 to increase TG excitability, showing that TREK1 and TREK2 control TG neuron excitability. To address the impact of this sensory neuron excitability increase, linked to TREK1 and TREK2 inhibition, we tested TREK1^{-/-}/TREK2^{-/-} mice for their susceptibility to a migraine-like phenotype. Migraine is associated with increased sensitivity to all sensory modalities and it appears that cutaneous allodynia can be used as a quantifiable marker of migraine disorder (Bates et al., 2010). Increase of basal mechanical hyperalgesia induced by TREK1 and TREK2 invalidation, to a similar level

compared to WT animals after ISDN injection, is in agreement with a KO-induced increase of sensory neuron excitability that is relevant to migraine (Brennan et al., 2013). Furthermore, trigeminal expression of MT2 in rats also induced a chronic facial allodynia which is directly linked to TG excitability and therefore relevant to migraine (Pradhan et al., 2014) (Kopruszinski et al., 2017) (Harris et al., 2017). Topiramate was previously shown to inhibit NO donor-induced acute or basal chronic hyperalgesia (Pradhan et al., 2014). We found that topiramate was able to partially reverse TREK1-TREK2 invalidation-induced hyperalgesia which is consistent with its action as a prophylactic migraine therapy (Pradhan et al., 2014). Therefore, the dysfunction of TREK1 and TREK2, and not TRESK alone, contributes to the increase of TG excitability which may lead to the altered pain processing associated with migraines. Together these results suggest that TREK1, TREK2 and TREK-TRESK heterodimers should be considered as new targets for migraine treatment.

An important remaining question is: how does TREK1 and TREK2 dysfunction lead to migraine phenotypes? Importantly, the TRESK-MT mutant has been found in migraine with aura phenotype (Lafrenière et al., 2010). Aura has been linked to cortical spreading depression (CSD) which precedes the activation of TG neurons (Nosedá and Burstein, 2013). TREK1 and TREK2 channel activity, by reducing TG excitability, may serve as a brake to prevent the pathological activation of TG neurons during the early stages of CSD. In patients expressing TRESK-MT this mechanism may be reduced or eliminated, enhancing the activation of TG neurons, thus leading to migraines. Fitting the model in which an increase in TG excitability is the primary underlying cause of headaches, the TRESK-MT proband described in the original Lafrenière paper (Lafrenière et al., 2010; OMIM #613656) also showed migraine headaches in isolation without a preceding aura.

Most importantly, this study led us to uncover an undescribed mechanism involving alternative translation initiation. We provide evidence that the 2 bp deletion observed for TRESK-MT introduces an in-frame start codon with the reference open reading frame of TRESK, allowing the formation of MT2, the TRESK fragment responsible for the increase in TG excitability. Translation initiation of most eukaryotic mRNAs follows a linear scanning mechanism where the 40S ribosome is recruited to the 5' cap structure

of the mRNA followed by downstream movement until an initiation codon is encountered (Kozak, 1999). In these cases, the translation initiation site is the first cap-proximal start codon for methionine (AUG). In most eukaryotic mRNA this first AUG is embedded into the Kozak consensus sequence [A/G]-XX-ATGG (Kozak, 1984a, b) (Jackson et al., 2010). However, if the first AUG is used inefficiently, some ribosomes read through the site without recognition; this leaky scanning can result in translation initiation at a downstream position (Thomas et al., 2008). This has been observed for TREK1, where the second strong ATI site allows the physiological formation of a TREK1 channel with a shorter N-terminus which leads to altered TREK1 ion selectivity (Thomas et al., 2008). Similar to what was seen with TREK1, the TRESK ATG at position +356 is embedded into the Kozak consensus sequence (**GCTATGG**), which may explain why this ATG can serve as an ATI. To further determine why the ATG at position +356 is able to serve as an ATI, we submitted the TRESK-MT sequence to TIS Miner and the ATGpr algorithms (Nishikawa et al., 2000) and both algorithms predicted that the ATG at position +356 is a strong start codon and it is the second possible start codon after ATG at position +1. Furthermore, we found that Kozak sequence mutation significantly reduced the TRESK-MT effect on TREK1 current. This indicates that leaky scanning may explain the generation of TRESK-MT2.

At the physiological level, ATI is thought to increase protein functional diversity as is also the case with RNA splicing. For example, it was recently shown in Osteogenesis Imperfecta (OI) disease, that a causative missense mutation of c.-14C>T of the cDNA encoding IFITM5 creates an upstream ATG (ACG at position -15 was mutated to give ATG) in the 5' UTR in frame with IFITM5 which can serve as an ATI site, resulting in addition of an N-terminal 15 AA sequence (Lazarus et al., 2014). Here, we find that an ATG embedded by a strong Kozak sequence, downstream of the ATG at position +1, can be put in frame by a frameshift mutation to induce the translation of a second truncated protein. In the present work, this second product was found to target TREK1 and TREK2 to increase TG neuron excitability and to produce mechanical allodynia, linking this mutant to migraine. This represents the first example where a frameshift mutation downstream of an ATG start codon at position +1 creates a new ORF allowing the production of a second product which is at the origin of a physiological disturbance. To see if this “frameshift mutation-

induced Alternative Translation Initiation” (fsATI) is a general phenomenon in TRESK, we predicted that any mutations before the stop codon TGA at position +427 that put the ATG at position +356 in frame would induce the formation of an MT2 that would lead to disease. Indeed, we demonstrate that another frameshift mutation, c.361dupT (Y121LfsX44), also leads to the formation of MT2 and is correlated to migraine (Clinvar, RCV000490385.1). It’s not possible to make any causal statements from this observation, but it is worth noting that this is the only other TRESK mutation which has been linked to a migraine phenotype. Together, this work shows that different frameshift mutations downstream of the first start codon can lead to ATI to produce a second protein which can carry the physiological function, suggesting that this mechanism may be widespread in nature and therefore needs to be considered when analyzing frameshift mutations linked to human disorders.

Materials and Methods

Molecular Biology, Cell Culture and Gene Expression

Channel DNA was used in the pIRES2eGFP, pcDNA3.1 and pCMV-HA vectors. HEK293T cells were maintained in DMEM with 5% FBS on poly-L-lysine-coated glass coverslips in 12 well plates. Cells were transiently co-transfected using Lipofectamine 2000 (Invitrogen) with a total of 1-1.6 µg of DNA total per 35 mm dish. When two genes were co expressed, a ratio of 1:1 DNA was used.

Primary cultures of mouse TG neurons

All mouse experiments were conducted according to national and international guidelines and have been approved by the local ethical committee (CIEPAL NCE). The C57BL/6J breeders were maintained on a 12 h light/dark cycle with constant temperature (23–24°C), humidity (45–50%), and food and water ad libitum at the animal facility of Valrose. TG tissues were collected from postnatal day 8 mice of either sex and treated with 2 mg/ml collagenase type II (Worthington) for ~2 hours, followed by 2.5 mg/ml trypsin for 15 min. Neurons were dissociated by triturating with fire-polished glass pipettes and seeded on polylysine/laminin coated coverslips. The DMEM-based culture medium contained 10% fetal bovine serum and 2mM GlutaMAX (Invitrogen). Neurons were transfected at 1 d in vitro (DIV) using Lipofectamine 2000 (Invitrogen). Transfected neurons were identified by the green fluorescence and patch clamp recordings were performed between DIV 3 and 5.

Knock-out mice

Mice lacking TREK1 and TREK2 were generated as described (Guyon et al., 2009). Null mutations were backcrossed against the C57BL/6J inbred strain for 10+ generations prior to establishing the breeding cages to generate subjects for this study. Age- and sex-matched C57BL/6J WT mice, aged 9-12 weeks, were obtained from Charles River Laboratories (Wilmington, MA).

Vector preparation

Adenovirus vector (DJ) encoding an IRES2EGFP or MT2-IRES2EGFP were used. Following linearization, this vector was recombined with the mouse version of the MT2 protein. The recombinant was amplified with PCR, and DNA sequencing was performed to verify the DNA sequence. Viral vectors were packaged and harvested by transfection of HEK 293T cells, followed by quantification of the viral titer through quantitative PCR. In addition, as a control, an adenovirus vector containing only the IRES2EGFP sequence was used.

Behavioral experiments

Animals

Experiments were performed on male Sprague Dawley rats (Janvier Labs) weighing 250 to 400 g (mean weight: 337 ± 16 g, 6 to 9 weeks old), and on male knock-out mice for TREK1 and TREK2 (weighting 20-25 g 7- to 13-weeks-old). Animals were housed in a 12 hour light-dark cycle with food and water available ad libitum. Animal procedures were approved by the Institutional Local Ethical Committee and authorized by the French Ministry of Research and the Spanish Ministry of Research according to the European Union regulations and the Directive 2010/63/EU (Agreements C061525 and 01550.03). Animals were sacrificed at experimental end points by CO2 euthanasia.

Drug administration and virus injection

For the topiramate experiment, mice were injected intraperitoneally with topiramate once at a dose of 30 mg/kg and mechanical nociception thresholds were assessed every 30 minutes for two hours after the injection.

The procedures of virus trigeminal injections are described by Long *et al.* (Long et al., 2017). Briefly, following general anesthesia with a cocktail of ketamine and xylazine (100 mg/kg and 10 mg/kg respectively in i.p), rats were shaved on the right side, which is the injected side, and placed on a warmed surgical plate. The site of injection was determined using a notch between the condylar process and the

ipsilateral angular process. The depth of injection was 9 mm. Antibiotics were used 5 days following injections. Viral vector suspension (10 μ L, 10^{11} transduction unit) containing 6 μ g/mL of Polybrene was injected slowly over 1 min. Rats in the experimental group (n=14) received 10 μ L of viral vector containing the MT2 protein sequence, while those in the control group (n=14) received the same amount of EGFP viral vector. Epifluorescence imaging and qPCR were performed to verify successful transduction of trigeminal ganglia by viral vector.

Mechanical sensitivity measurements

The face mechanical sensitivity was measured using calibrated von Frey filaments (Bioseb, France). Unrestrained rats placed in individual plastic boxes on top of a wire surface were trained over one week to stimulation on the periorbital area, following a progressive protocol, starting with non-noxious filaments during the first 3 days of training. The face withdrawal force threshold (g) was determined by the filament evoking at least three responses over five trials, starting with lower force filaments. Basal values were determined 2 days before experiments.

The hindpaw mechanical sensitivity was evaluated with a dynamic plantar aesthesiometer (Ugo Basile, Italy). Unrestrained mice were placed in 10 individual plastic boxes on top of a wire surface. The mouse hindpaw was submitted to a force ramp up to 7.5 g during 10 s, the paw withdrawal force threshold (g) was assessed in three consecutive trials with at least 3–5 min between the trials and averaged to select animals. Basal values were determined 2 days before experiments.

Migraine rodent models

The rodent model of NO-induced migraine was induced by intraperitoneal (i.p.) injection of ISDN (Risordan®, Sanofi) at 10mg/kg, a long-lasting NO donor. The vehicle control used in these experiments was 0.9% saline. The acute mechanical allodynia induced by a single ISDN injection was followed on the hindpaw for mice and on the face for rats before (basal value) and for 3 hours after injection, every 30 minutes. Chronic mechanical allodynia was induced by a single daily injection of ISDN during 4 days. The

hindpaw extra-cephalic mechanical sensitivity was measured each day before the ISDN i.p. injection for mice. Topiramate was tested on chronic mechanical allodynia on the 5th day and effects were followed every 30 min during 2 hours after injection in mice.

Electrophysiology

HEK 293T cell electrophysiology was performed 24-72 h after Lipofectamine transfection in solution containing (in mM): 145 mM NaCl, 4 mM KCl, 1 mM MgCl₂, 2 mM CaCl₂ and 10 mM HEPES. For co-expression of K₂P channels and mutant channels, a DNA ratio of 1:1 was used. Glass pipettes of resistance between 3 and 6 MΩ were filled with intracellular solution containing (in mM): 140 KCl, 10 Hepes, 5 EGTA, 3 MgCl₂, pH 7.4. Cells were patch clamped using an Axopatch 200A (Molecular Devices) amplifier in the whole cell mode. Currents were elicited by voltage-ramps (from -100 to 100 mV, 1s in duration) and the current density was calculated at 0 mV.

Oocyte two-electrode voltage clamp electrophysiology was performed in a 0.3-mL perfusion chamber; a single oocyte was impaled with two standard microelectrodes (1–2.5 MΩ resistance) filled with 3 M KCl, and maintained under voltage clamp using a Dagan TEV 200 amplifier in standard ND96 solution [96 mM NaCl, 2 mM KCl, 1.8 mM CaCl₂, 2 mM MgCl₂, 5 mM Hepes pH 7.4 with NaOH]. For the high K solution contained 80 mM K⁺, 78 mM NaCl was replaced by KCl. Stimulation of the preparation, data acquisition, and analysis were performed using pClamp software (Molecular Devices).

Neuronal excitability was studied in small-diameter TG neurons transfected with 1 μg of the pIRES2EGFP vector containing the X insert in which there is no N-terminal tag on the insert and EGFP is co-translated as a transfection marker or the pIRES2EGFP control plasmid with Lipofectamine 2000. Extracellular solution contained (in mM): 135 NaCl, 5 KCl, 2 CaCl₂, 1 MgCl₂, 5 HEPES, 10 glucose, pH 7.4 with NaOH, 310 mOsm. The pipette solution contained the following (in mM): 140 K-gluconate, 10 NaCl, 2 MgCl₂, 5 EGTA, 10 HEPES, 2 ATP-Mg, 0.3 GTP-Na, 1 CaCl₂ pH 7.3 with KOH, 290 mOsm. Recording pipettes had < 4.5 MΩ resistance. Series resistance (<20 MΩ) was not compensated. Signals were filtered

at 10 kHz and digitized at 20 kHz. After establishing whole-cell access, membrane capacitance was determined with amplifier circuitry. The amplifier was then switched to current-clamp mode to measure resting membrane potential (V_{rest}). Neurons were excluded from analysis if the V_{rest} was higher than -40 mV or if the input resistance was smaller than 200 M Ω . To test neuronal excitability, neurons were held at V_{rest} and injected with 1 s depolarizing currents in 25 pA incremental steps until at least 1 action potential (AP) was elicited.

Trigeminal neurons RNA extraction and reverse transcription

Total RNA was isolated from trigeminal neurons in suspension using a Nucleospin RNA Plus XS kit (from MACHEREY-NAGEL GmbH & Co. KG) according to the manufacturer's protocols and 1 μ g of RNA was reverse transcribed (with 10 nM random hexamers for 5 min at 65°C, then with 10 mM DTT, 0.5 mM each dNTP, 100 U SuperScript II (Invitrogen) 42°C for 50 min). Subsequently, the cDNA was quantified by qPCR with PowerUp SYBR Green Master Mix (Thermo Fisher).

Single cell reverse transcription

The procedures of single cell RT-PCR are adapted from Johansen *et al.* (Johansen et al., 1995). The content of each cell was aspirated into the patch pipette by applying negative pressure. The flow of the cytosol in the pipette as well as the aspiration of the nucleus was controlled under the microscope. Only cell samples which included the nucleus were investigated in the present study.

The pipette was then released from the holder and mounted on a syringe to expel its content into a test tube. To the ~6.5 μ L of the pipette-content expelled into the test tube was added 3.5 μ L of a solution containing random hexamers (Invitrogen, 5 μ M final concentration), dithiothreitol (DTT, final concentration 10 mM), the four deoxyribonucleotide triphosphates (dNTP, Thermo Fisher, final 0,5 mM each), 20 U ribonuclease inhibitor (Promega), and 100 U Moloney murine leukemia virus reverse transcriptase (Invitrogen).

The total 10 μ L reaction was incubated for 1h at 35°C for synthesis of single stranded cDNA, and then kept on ice until PCR.

PCR amplification and quantification

Semi-quantitative PCR were performed to determine the relative levels of TREK1, TREK2, and TRESK after RNA extraction and reverse transcription using primers described below. qPCR (10 μ L) was performed using the aforementioned reverse-transcribed cDNA (4 μ L) and the primers for TREK1 (forward: catcttcacctctgttgctg, reverse : atcatgctcagaacagctgc, 240 pb), TREK2 (forward : aacagtggttgccatctcg, reverse: ccagcaaagaagaaggcact, 276 pb), TRESK (forward : ctgcttcctttgctgctg, reverse : aagaagagagcgcctcaggaa, 256 pb) and GAPDH (forward : cctggagaaacctgccaagtatga, reverse : tgctgtgaagtcgcaggaga) as a reference. After initial denaturation at 95°C for 15 seconds, 40 cycles of amplification (95°C for 15 seconds and 60°C for 1 minute) were performed.

Quantitative PCR were performed to determine the levels of GFP after inoculation of adenovirus vectors containing GFP MT2 sequences into trigeminal ganglia using the same protocol with specific primers for the GFP (forward : aagctgaccctgaagttcatctgc, reverse : cttgtagttgccgctccttgaa).

Analysis were made using the GAPDH as the housekeeping gene along with the 2- $\Delta\Delta$ Ct Calculation Method.

Western blot analysis

24 to 48 hours after transfection using 1 μ g DNA with Lipofectamine 2000, HEK 293T cells were homogenized in PBS containing saponin (0.5% w/v), Triton X-100 (0.5% w/v) and protease inhibitors (Roche Diagnostics, Basel, Switzerland). Lysates were clarified by centrifugation at 20 000 g for 30 min. Proteins were separated on 10% SDS polyacrylamide gel and blotted onto nitrocellulose membrane (Hybond-C extra, Amersham Biosciences, Freiburg, Germany). Detection was carried out using mouse monoclonal antibody clone HA-7 against the HA epitope (Sigma).

Immunocytochemistry

Transfected neurons on coverslips were fixed with PBS containing 4% paraformaldehyde for 15 minutes at room temperature (RT), then permeabilized with PBS and 0,1% Triton X-100 (PBST) and blocked for 1h with 5% horse serum (HS) in PBST. Primary and secondary antibodies were diluted in PBST and 5% HS and incubated for 1h at RT. Three 5-min washes with PBST were carried out between each incubation step and at the end of the procedure. Coverslips were mounted in Dako Fluorescent Mounting medium (Dako Corporation, Carpinteria, CA, USA). The following antibodies were used: rabbit anti-TREK1 and TREK2 (Blin et al., 2016), anti-TRESK (ab96868, abcam) conjugated with Cy3 (ab146452, abcam), Cy5 (ab146454, abcam) and Atto 488 (Sigma) respectively. Microscopy analysis and data acquisition were carried out with an Axioplan 2 Imaging Microscope (Zeiss®).

Single Molecule Pulldown

For SiMPull experiments, a DNA ratio of 1:1 was used. 24 hours after transfection, HEK 239T cells were harvested from coverslips by incubating with Ca²⁺-free PBS buffer for 20-30 minutes followed by gentle pipetting. Cells were lysed in buffer containing (in mM): 150 NaCl, 10 Tris pH 7.5, 1 EDTA, protease inhibitor cocktail (Thermo Scientific) and 1.5% IGEPAL (Sigma) or 1% DDM (Sigma). After 30-60 minute incubation at 4°, lysate was centrifuged for 20 minutes at 12,500 g and the supernatant was collected. Coverslips passivated with PEG (~99%)/ biotin-PEG (~1%) and treated with NeutrAvidin (Pierce) were prepared as described (Jain et al., 2012). 15 nM biotinylated anti-HA antibody (clone 16B12, BioLegend) was applied for 20 minutes and then washed out. Antibody dilutions and washes were done in T50 buffer with BSA containing (in mM): 50 NaCl, 10 Tris pH 7.5, and 0.1 mg/mL BSA. Lysate, diluted in lysis buffer containing 0.04% IGEPAL, was then applied to the chamber and washed away following brief incubation (~2 minutes). Single molecules were imaged using a 488 nm Argon laser on a total internal reflection fluorescence microscope with a 60x objective (Olympus). We recorded the emission light after an additional 3x magnification and passage through a double dichroic mirror and an emission filter (525/50 for GFP) with a back-illuminated EMCCD camera (Andor iXon DV-897 BV). Movies of 250-500 frames were acquired at frame rates of 10–30 Hz. The imaged area was 13 x 13 μm². At least 5 movies were recorded

for each condition and data was analyzed using custom software. Multiple independent experiments were performed for each condition. Representative data sets are presented to quantitatively compare conditions tested on the same day.

Acknowledgments

We thank Rainer Waldman, Bernard Mari, Kevin Le Brigand, Eric Lingueglia, Michel Lanteri-Minet, Emile Piquet and Maximillian Furthauer for helpful discussion. The work was supported by a grant to GS by the ATIP-AVENIR funds and the Fondation pour la Recherche Medicale (Equipe labellisée FRM 2017, FRM DEQ20170336753) as well as grants to GS and FL from the Agence Nationale de la Recherche (Laboratory of Excellence “Ion Channel Science and Therapeutics“, grant ANR-11-LABX-0015-01 and ANR Dynaselect, Grant ANR-14-CE13-0010). We thank A. Monteil and C. Lemmers from the Vectorology facility, PVM, Biocampus Montpellier, CNRS UMS3426 for virus production. The microscopy was done in the Prism facility, “Plateforme PRISM – IBV- CNRS UMR 7277- INSERM U1091-UNS». Magali Mondin is acknowledged. Histopathological analyses were performed on the Experimental Histopathology Platform of iBV, CNRS UMR7277-INSERM U1091-UNS». The help of Samah REKIMA is acknowledged.

References:

- Alloui, A., Zimmermann, K., Mamet, J., Duprat, F., Noël, J., Chemin, J., Guy, N., Blondeau, N., Voilley, N., Rubat-Coudert, C., *et al.* (2006). TREK-1, a K⁺ channel involved in polymodal pain perception. *EMBO J* 25, 2368-2376.
- Andres-Enguix, I., Shang, L., Stansfeld, P.J., Morahan, J.M., Sansom, M.S., Lafrenière, R.G., Roy, B., Griffiths, L.R., Rouleau, G.A., Ebers, G.C., *et al.* (2012). Functional analysis of missense variants in the TRESK (KCNK18) K channel. *Sci Rep* 2, 237.
- Bates, E.A., Nikai, T., Brennan, K.C., Fu, Y.H., Charles, A.C., Basbaum, A.I., Ptáček, L.J., and Ahn, A.H. (2010). Sumatriptan alleviates nitroglycerin-induced mechanical and thermal allodynia in mice. *Cephalalgia* 30, 170-178.
- Bautista, D.M., Sigal, Y.M., Milstein, A.D., Garrison, J.L., Zorn, J.A., Tsuruda, P.R., Nicoll, R.A., and Julius, D. (2008). Pungent agents from Szechuan peppers excite sensory neurons by inhibiting two-pore potassium channels. *Nat Neurosci* 11, 772-779.
- Blin, S., Ben Soussia, I., Kim, E.J., Brau, F., Kang, D., Lesage, F., and Bichet, D. (2016). Mixing and matching TREK/TRAAK subunits generate heterodimeric K₂P channels with unique properties. *Proc Natl Acad Sci U S A* 113, 4200-4205.
- Brennan, K.C., Bates, E.A., Shapiro, R.E., Zyuzin, J., Hallows, W.C., Huang, Y., Lee, H.Y., Jones, C.R., Fu, Y.H., Charles, A.C., and Ptáček, L.J. (2013). Casein kinase I δ mutations in familial migraine and advanced sleep phase. *Sci Transl Med* 5, 183ra156, 181-111.
- Dobler, T., Springauf, A., Tovornik, S., Weber, M., Schmitt, A., Sedlmeier, R., Wischmeyer, E., and Döring, F. (2007). TRESK two-pore-domain K⁺ channels constitute a significant component of background potassium currents in murine dorsal root ganglion neurones. *J Physiol* 585, 867-879.
- Guo, Z., Liu, P., Ren, F., and Cao, Y.Q. (2014). Nonmigraine-associated TRESK K⁺ channel variant C110R does not increase the excitability of trigeminal ganglion neurons. *J Neurophysiol* 112, 568-579.
- Guyon, A., Tardy, M.P., Rovère, C., Nahon, J.L., Barhanin, J., and Lesage, F. (2009). Glucose inhibition persists in hypothalamic neurons lacking tandem-pore K⁺ channels. *J Neurosci* 29, 2528-2533.
- Harris, H.M., Carpenter, J.M., Black, J.R., Smitherman, T.A., and Sufka, K.J. (2017). The effects of repeated nitroglycerin administrations in rats; modeling migraine-related endpoints and chronification. *J Neurosci Methods* 284, 63-70.
- Hwang, E.M., Kim, E., Yarishkin, O., Woo, D.H., Han, K.S., Park, N., Bae, Y., Woo, J., Kim, D., Park, M., *et al.* (2014). A disulphide-linked heterodimer of TWIK-1 and TREK-1 mediates passive conductance in astrocytes. *Nat Commun* 5, 3227.
- Jackson, R.J., Hellen, C.U., and Pestova, T.V. (2010). The mechanism of eukaryotic translation initiation and principles of its regulation. *Nat Rev Mol Cell Biol* 11, 113-127.
- Jain, A., Liu, R., Xiang, Y.K., and Ha, T. (2012). Single-molecule pull-down for studying protein interactions. *Nat Protoc* 7, 445-452.
- Johansen, F.F., Lambolez, B., Audinat, E., Bochet, P., and Rossier, J. (1995). Single cell RT-PCR proceeds without the risk of genomic DNA amplification. *Neurochem Int* 26, 239-243.
- Kochetov, A.V. (2008). Alternative translation start sites and hidden coding potential of eukaryotic mRNAs. *Bioessays* 30, 683-691.

Kopruszinski, C.M., Xie, J.Y., Eyde, N.M., Remeniuk, B., Walter, S., Stratton, J., Bigal, M., Chichorro, J.G., Dodick, D., and Porreca, F. (2017). Prevention of stress- or nitric oxide donor-induced medication overuse headache by a calcitonin gene-related peptide antibody in rodents. *Cephalalgia* 37, 560-570.

Kozak, M. (1984a). Compilation and analysis of sequences upstream from the translational start site in eukaryotic mRNAs. *Nucleic Acids Res* 12, 857-872.

Kozak, M. (1984b). Point mutations close to the AUG initiator codon affect the efficiency of translation of rat preproinsulin in vivo. *Nature* 308, 241-246.

Kozak, M. (1999). Initiation of translation in prokaryotes and eukaryotes. *Gene* 234, 187-208.

Lafrenière, R.G., Cader, M.Z., Poulin, J.F., Andres-Enguix, I., Simoneau, M., Gupta, N., Boisvert, K., Lafrenière, F., McLaughlan, S., Dubé, M.P., *et al.* (2010). A dominant-negative mutation in the TRESK potassium channel is linked to familial migraine with aura. *Nat Med* 16, 1157-1160.

Landrum, M.J., Lee, J.M., Benson, M., Brown, G., Chao, C., Chitipiralla, S., Gu, B., Hart, J., Hoffman, D., Hoover, J., *et al.* (2016). ClinVar: public archive of interpretations of clinically relevant variants. *Nucleic Acids Res* 44, D862-868.

Lazarus, S., McInerney-Leo, A.M., McKenzie, F.A., Baynam, G., Broley, S., Cavan, B.V., Munns, C.F., Pruijs, J.E., Sillence, D., Terhal, P.A., *et al.* (2014). The IFITM5 mutation c.-14C > T results in an elongated transcript expressed in human bone; and causes varying phenotypic severity of osteogenesis imperfecta type V. *BMC Musculoskelet Disord* 15, 107.

Lek, M., Karczewski, K.J., Minikel, E.V., Samocha, K.E., Banks, E., Fennell, T., O'Donnell-Luria, A.H., Ware, J.S., Hill, A.J., Cummings, B.B., *et al.* (2016). Analysis of protein-coding genetic variation in 60,706 humans. *Nature* 536, 285-291.

Lengyel, M., Czirják, G., and Enyedi, P. (2016). Formation of Functional Heterodimers by TREK-1 and TREK-2 Two-pore Domain Potassium Channel Subunits. *J Biol Chem* 291, 13649-13661.

Levitz, J., Royal, P., Comoglio, Y., Wdziekonski, B., Schaub, S., Clemens, D.M., Isacoff, E.Y., and Sandoz, G. (2016). Heterodimerization within the TREK channel subfamily produces a diverse family of highly regulated potassium channels. *Proc Natl Acad Sci U S A* 113, 4194-4199.

Liu, P., Xiao, Z., Ren, F., Guo, Z., Chen, Z., Zhao, H., and Cao, Y.Q. (2013). Functional analysis of a migraine-associated TRESK K⁺ channel mutation. *J Neurosci* 33, 12810-12824.

Long, H., Liao, L., Zhou, Y., Shan, D., Gao, M., Huang, R., Yang, X., and Lai, W. (2017). A novel technique of delivering viral vectors to trigeminal ganglia in rats. *Eur J Oral Sci* 125, 1-7.

Morenilla-Palao, C., Luis, E., Fernández-Peña, C., Quintero, E., Weaver, J.L., Bayliss, D.A., and Viana, F. (2014). Ion channel profile of TRPM8 cold receptors reveals a role of TASK-3 potassium channels in thermosensation. *Cell Rep* 8, 1571-1582.

Nishikawa, T., Ota, T., and Isogai, T. (2000). Prediction whether a human cDNA sequence contains initiation codon by combining statistical information and similarity with protein sequences. *Bioinformatics* 16, 960-967.

Nosedá, R., and Burstein, R. (2013). Migraine pathophysiology: anatomy of the trigeminovascular pathway and associated neurological symptoms, CSD, sensitization and modulation of pain. *Pain* 154 Suppl 1.

Noël, J., Zimmermann, K., Busserolles, J., Deval, E., Alloui, A., Diochot, S., Guy, N., Borsotto, M., Reeh, P., Eschalier, A., and Lazdunski, M. (2009). The mechano-activated K⁺ channels TRAAK and TREK-1 control both warm and cold perception. *EMBO J* 28, 1308-1318.

- Pradhan, A.A., Smith, M.L., McGuire, B., Tarash, I., Evans, C.J., and Charles, A. (2014). Characterization of a novel model of chronic migraine. *Pain* 155, 269-274.
- Sandoz, G., Levitz, J., Kramer, R.H., and Isacoff, E.Y. (2012). Optical control of endogenous proteins with a photoswitchable conditional subunit reveals a role for TREK1 in GABA(B) signaling. *Neuron* 74, 1005-1014.
- Sano, Y., Inamura, K., Miyake, A., Mochizuki, S., Kitada, C., Yokoi, H., Nozawa, K., Okada, H., Matsushime, H., and Furuichi, K. (2003). A novel two-pore domain K⁺ channel, TRESK, is localized in the spinal cord. *J Biol Chem* 278, 27406-27412.
- Thomas, D., Plant, L.D., Wilkens, C.M., McCrossan, Z.A., and Goldstein, S.A. (2008). Alternative translation initiation in rat brain yields K2P2.1 potassium channels permeable to sodium. *Neuron* 58, 859-870.
- Ulbrich, M.H., and Isacoff, E.Y. (2007). Subunit counting in membrane-bound proteins. *Nat Methods* 4, 319-321.
- Verkest, C., Piquet, E., Diochot, S., Dauvois, M., Lanteri-Minet, M., Lingueglia, E., and Baron, A. (2018). Effects of systemic inhibitors of acid-sensing ion channels 1 (ASIC1) against acute and chronic mechanical allodynia in a rodent model of migraine. *Br J Pharmacol*.
- Walsh, Y., Leach, M J, Veale, E., and Mathie, A. (2016). Identified regions of TREK and TRESK two pore domain potassium channels critical for inhibition by sipatragine and lamotrigine. In *Proceedings of The Physiological Society*, T.P. Socitey, ed. (Dublin, **Proc Physiol Soc**).
- Wood, H. (2010). Migraine: Familial migraine with aura is associated with a mutation in the TRESK potassium channel. *Nat Rev Neurol* 6, 643.
- Yamamoto, Y., Hatakeyama, T., and Taniguchi, K. (2009). Immunohistochemical colocalization of TREK-1, TREK-2 and TRAAK with TRP channels in the trigeminal ganglion cells. *Neurosci Lett* 454, 129-133.
- Yan, J., and Dussor, G. (2014). Ion channels and migraine. *Headache* 54, 619-639.

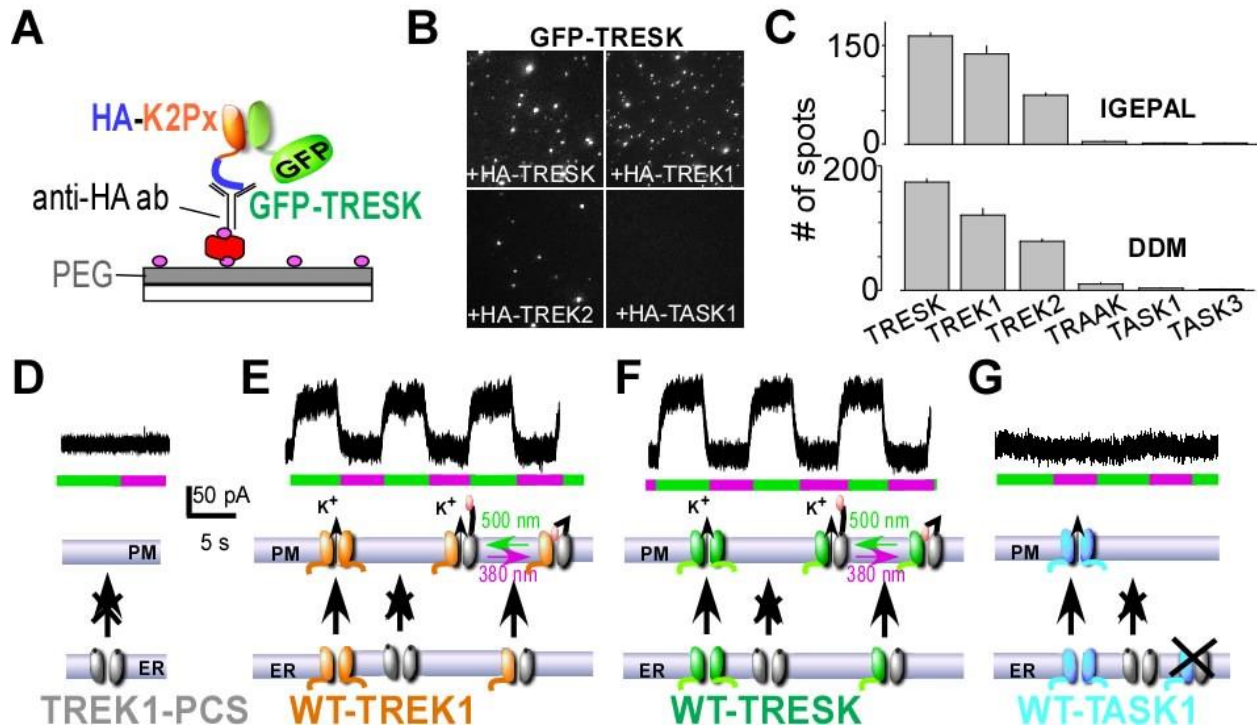


Figure 1: TRESK heteromerizes physically and functionally with TREK1 and TREK2. (A) Schematic of single molecule pulldown (SiMPull) of GFP-TRESK. HEK 293T cells expressing GFP-TRESK and an HA-tagged K2P channel (“HA-K2Px”) were lysed and then immobilized on a PEG-passivated coverslip conjugated to a biotinylated anti-HA antibody. (B-C) Representative images (IGEPAL) and summary bar graphs with 2 different detergents, IGEPAL and DDM, showing pulldown of GFP-TRESK by HA-TRESK, HA-TREK1 or HA-TREK2, but not by HA-TASK1, HA-TASK3, or HA-TRAAK. (D-G) Co-expression of TREK1-PCS with WT-TREK1 produces a heteromeric channel that traffics from the endoplasmic reticulum (ER) to the plasma membrane (PM) and which can be light-gated due to attachment of a photoswitchable blocker to the TREK1-PCS. TREK1-PCS expression alone does not produce any photoswitchable current (D), but co-expression of TREK1 (E) or TRESK (F), but not TASK1 (G) leads to a photoswitchable current indicating that TREK1-TRESK form functional heteromers but there is no functional assembly of TREK1 and TASK1.

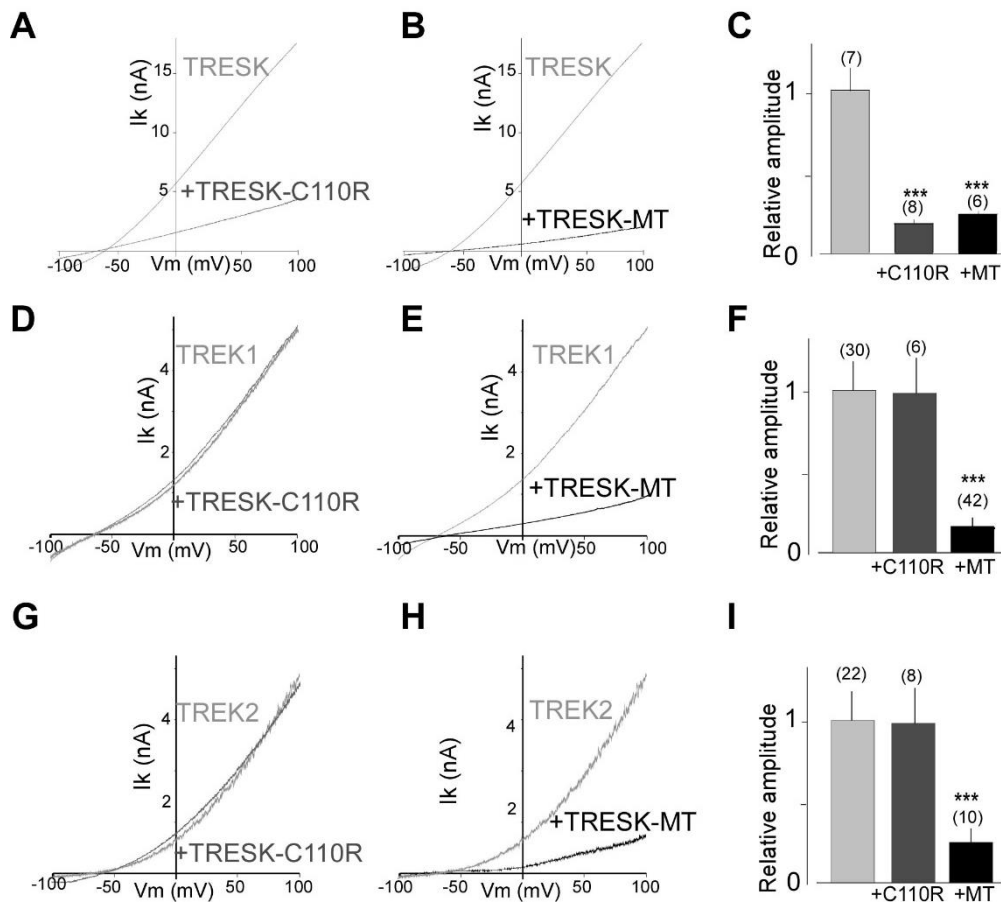


Figure 2. TRESK-MT, but not TRESK-C110R, acts as a dominant negative on TREK1 and TREK2 channels. (A, B) Representative traces showing the effect of TRESK-C110R (A) and TRESK-MT (B) co-expression on TRESK current in HEK 293T cells. Currents were elicited by voltage-ramps (from -100 to 100 mV, 1s duration). (C) Bar graph summarizing the relative TRESK current amplitude at 0 mV for TRESK when TRESK-C110R and TRESK-MT are or not coexpressed. (D-F) Same as (A-C) for TREK1. (G-I) same as (A-C) for TREK2. The numbers of cells tested are indicated in parentheses. Student's *t* test (***) $P < 0.001$).

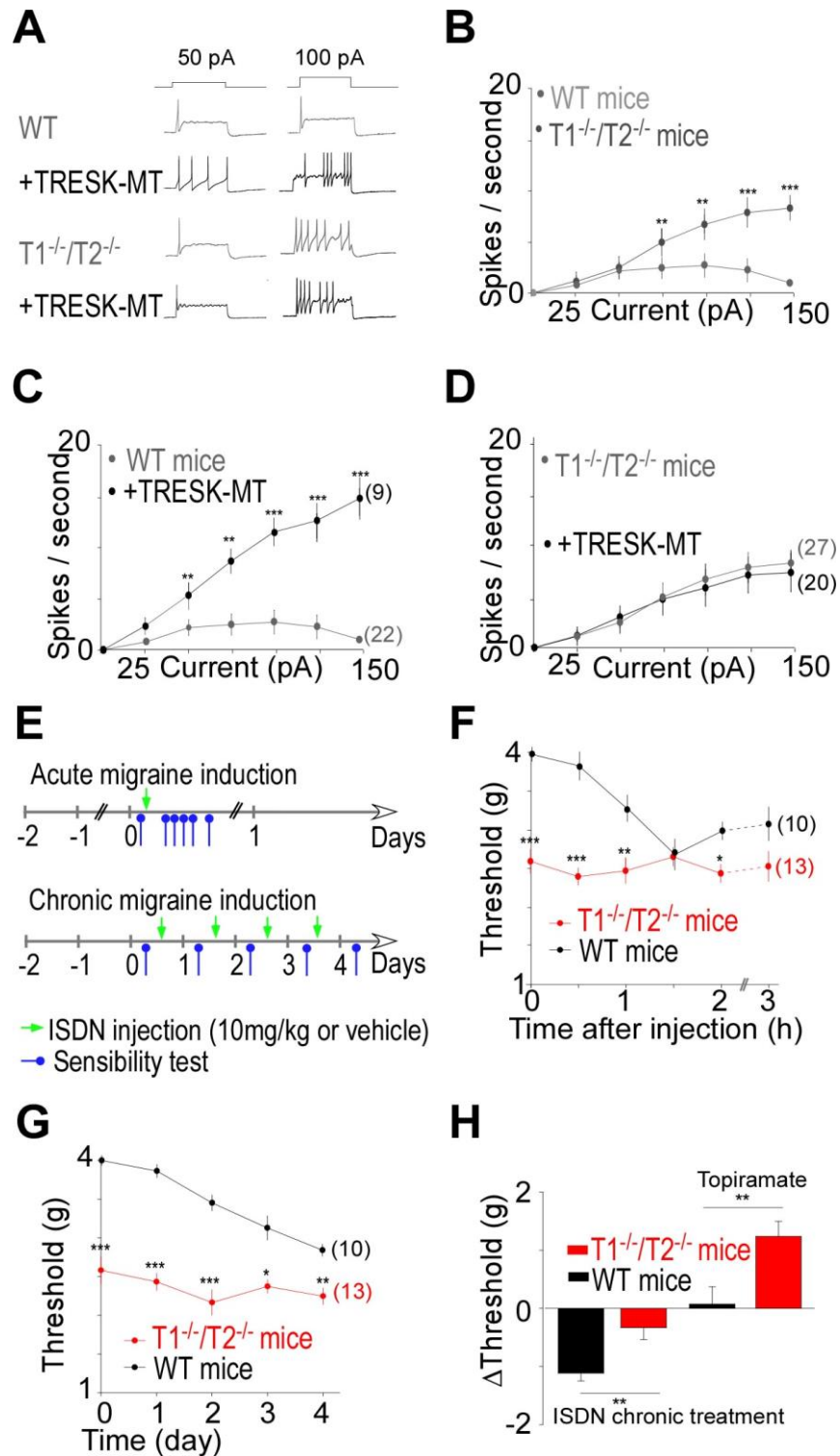


Figure 3. TREK1 and TREK2 invalidation increases sensory neuron excitability and mechanical pain perception (A-D) TREK1^{-/-}/TREK2^{-/-} TG neurons are more excitable than WT TG neurons and are not sensitive to TRESK-MT overexpression. **(A)** Representative traces of action potentials (spikes) generated

by incremental depolarizing current injections in small-diameter TG neurons. **(B)** Input-output plots of spike frequency in response to 1s depolarizing current injection in untransfected, small TG neurons from WT and TREK1^{-/-}/TREK2^{-/-} double KO mice. **(C, D)** TRESK-MT acts as a dominant negative on TREK1 and TREK2 channels to increase excitability of TG neurons. Input-output plots of the spike frequency in response to 1s depolarizing current injection in transfected small TG neurons from WT **(C)** and TREK1^{-/-}/TREK2^{-/-} double KO mice **(D)**, show that an increase in excitability elicited by TRESK-MT is observed in WT, but not T1^{-/-}/T2^{-/-} neurons. The numbers of tested cells are indicated in parentheses. Student's *t* test (**P* < 0.05, ***P* < 0.01, ****P* < 0.001). **(E-H)** TREK1^{-/-}/TREK2^{-/-} double knockout animals present a migraine-like hypersensitivity to mechanical stimuli. **(E)** Schematic of experimental behavioral paradigms. Green arrows represent the injection of ISDN, a known migraine trigger. Blue arrows represent the measurement of mechanical sensitivity. **(F)** Paw withdrawal mechanical threshold, assessed after the first ISDN injection, were significantly decreased in double knockout animals and remained less than WT for the first 1.5 hrs following ISDN injection. **(G)** Mechanical responses, assessed prior to and after chronic ISDN injections, were significantly decreased in double knockout animals. **(H)** Comparison of the Paw withdrawal mechanical threshold before and after topiramate injection. Mechanical responses were assessed before and 2 hours after topiramate injection from WT and TREK1^{-/-}/TREK2^{-/-} double knockout ISDN-non treated mice. Numbers of mice tested are indicated in parentheses, Student's *t* test to compare WT vs TREK1^{-/-}/TREK2^{-/-} mice (**P* < 0.05, ***P* < 0.01, ****P* < 0.001).

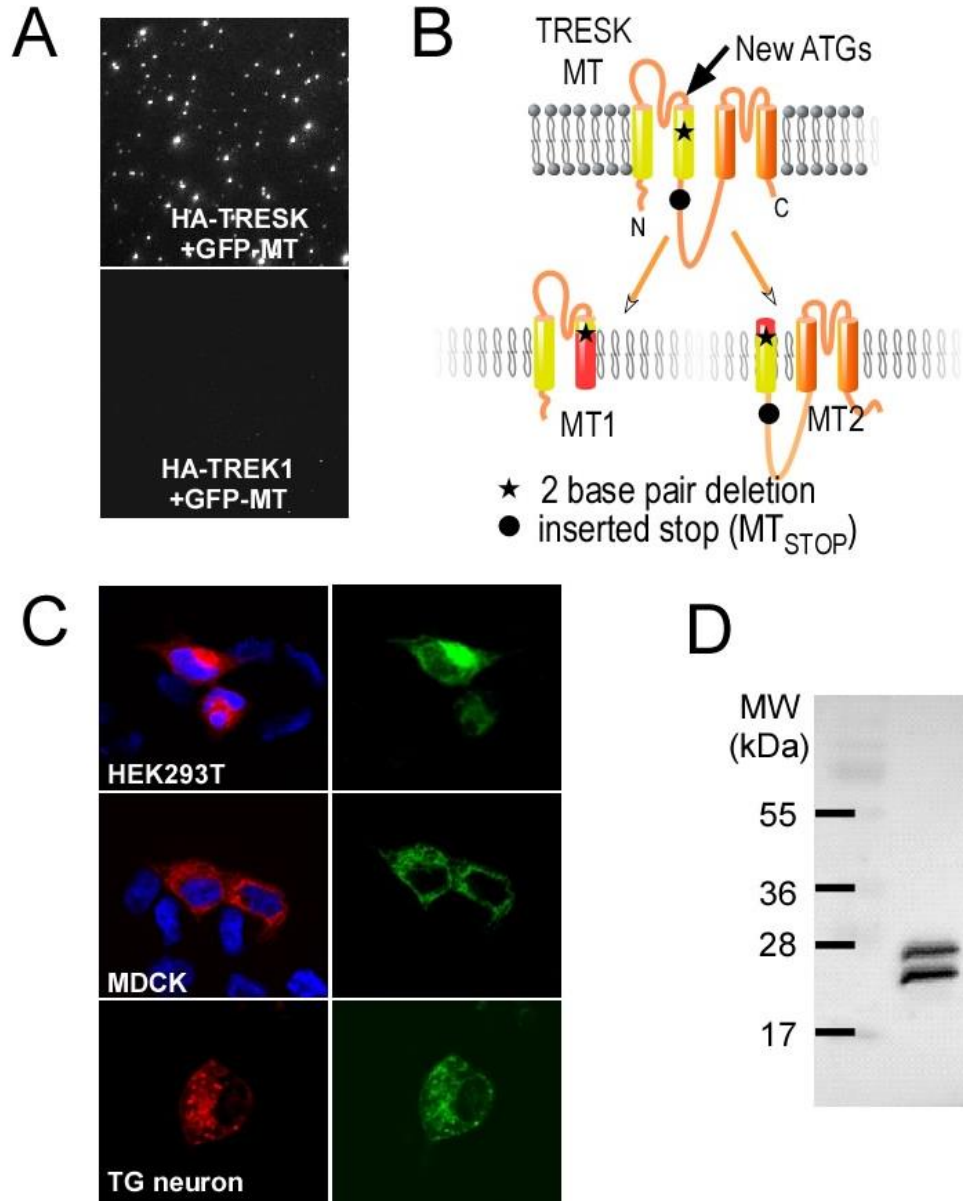


Figure 4. TRESK-MT induces the translation of a second protein, MT2. (A) Representative images from SiMPull experiments showing that GFP-TRESK-MT can be pulled down by HA-TRESK but not by HA-TREK1. (B) Cartoon showing the membrane topology of TRESK and the expected products induced by ATI in the TRESK-MT mutation. The region corresponding to aberrant sequences are shown in red. (C) Co-synthesis of mCherry-MT1 and MT2-GFP products from the mCherry-TRESK-MT-GFP cDNA in HEK 293T cells (top), MDCK (middle) and TG neurons (bottom). DAPI nuclear stain is shown in blue.

(D) Western blot against HA-TRESK-MT-HA probed with anti-HA antibodies from HEK 293T cells lysate.

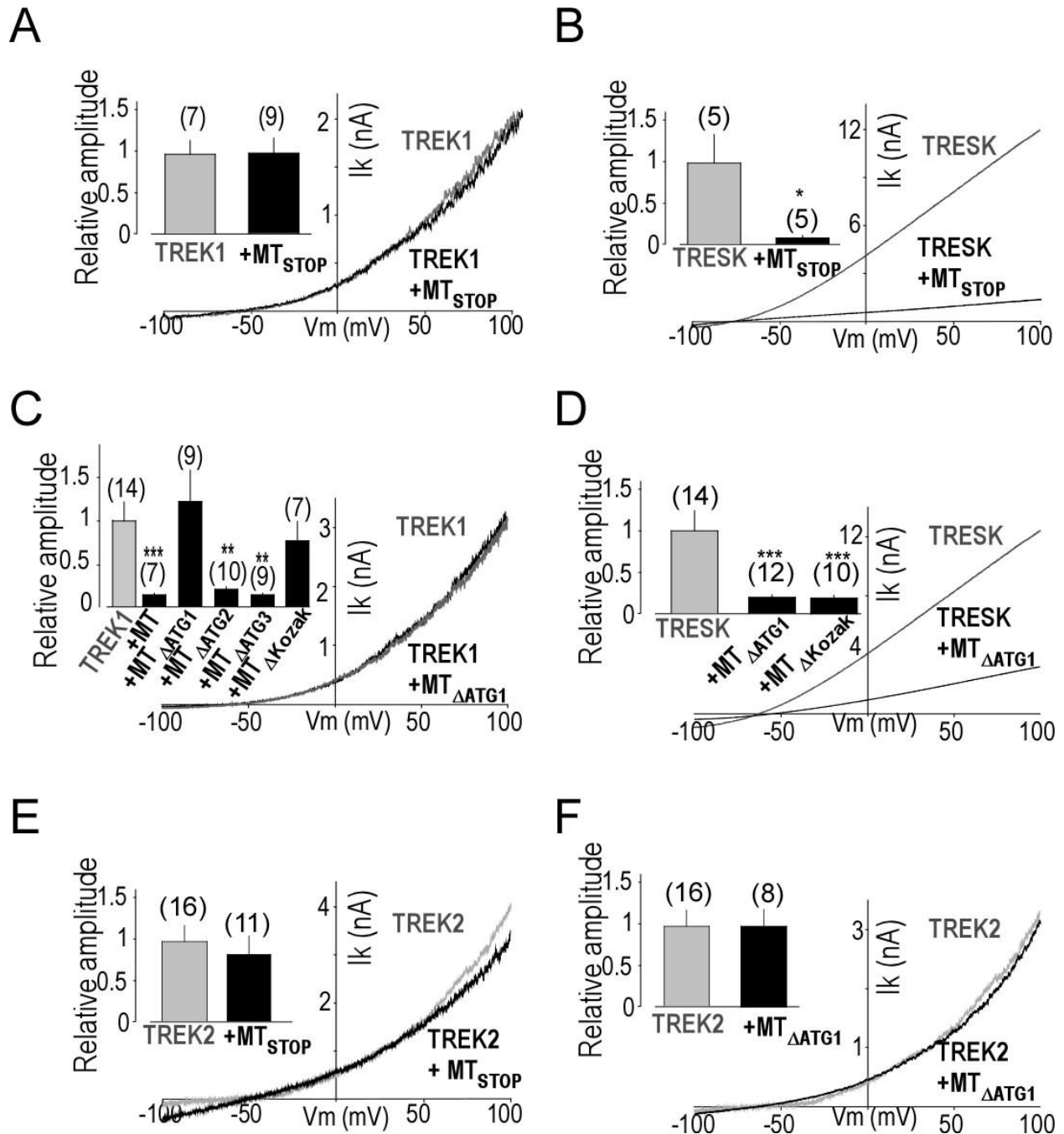


Figure 5. MT2 mediates TREK1 inhibition. (A) Representative traces showing the effect of introduction of a STOP codon at the beginning of the MT2 ORF within the 2-3 loop (TRESK-MT_{STOP}) on TREK1 current in HEK 293T cells. Inset shows a summary of TREK1 relative current densities when TRESK-MT_{STOP} is coexpressed. (B) Representative traces showing the effect of TRESK-MT_{STOP} on TRESK current. Insets, TRESK relative current densities when TRESK-MT_{STOP} is coexpressed. (C) Representative traces

showing the effect of introduction of a mutation of ATG at position +356 (Δ ATG1) on TREK1 current and summary bar graph showing the effect of mutation of candidate alternative start codons (Δ ATG1, Δ ATG2, or Δ ATG3) and mutation of the Kozak sequence surrounding ATG1 (Δ Kozac) in TRESK-MT. Currents were elicited by voltage-ramps (from -100 to 100 mV, 1s duration). **(D)** Representative traces showing the effect of TRESK-MT $_{\Delta$ ATG1 on TRESK current. Insets, TRESK relative current densities when TRESK-MT $_{\Delta$ ATG1 is coexpressed. **(E, F)** same as (A, C) for TREK2. The numbers of cells tested are indicated in parentheses. Student's *t* test (**P* < 0.05, ***P* < 0.01, ****P* < 0.001) shows the difference between TREK1 or TRESK or TREK2 and TREK1 or TRESK or TREK2 when co-expressed with different TRESK-MT constructs.

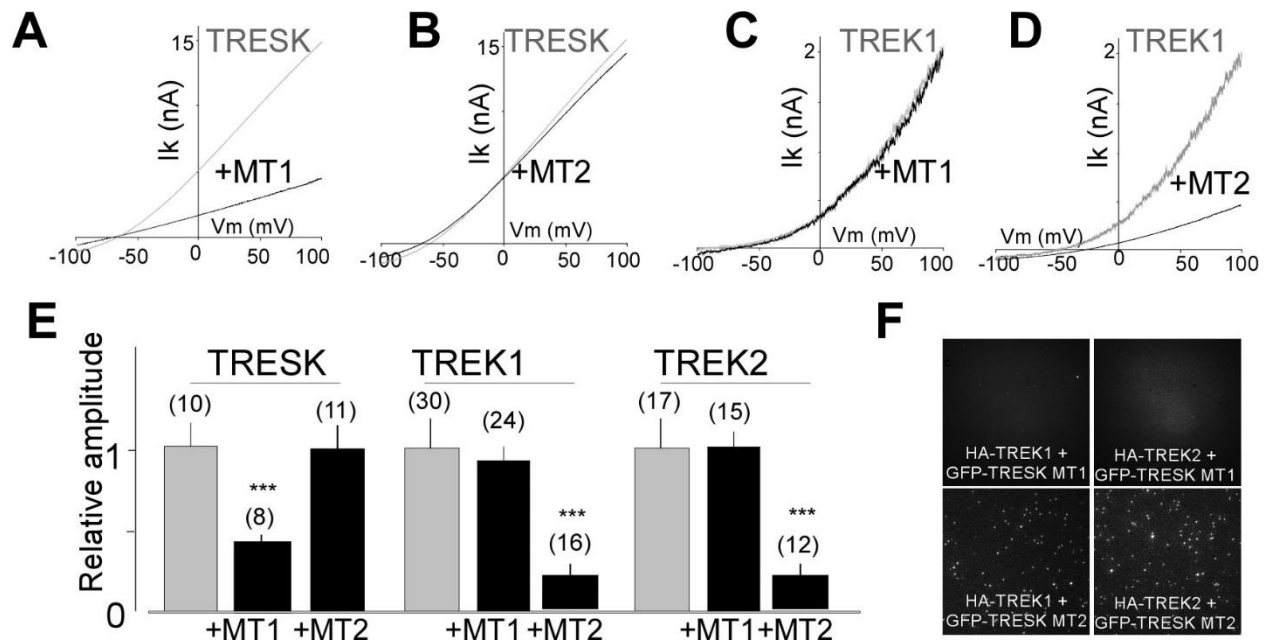


Figure 6. MT1 acts as dominant negative on TRESK whereas MT2 acts as a dominant negative on TREK1 and TREK2 channels. (A-D) Representative traces showing the effect of TRESK-MT1 (A and C) or TRESK-MT2 (B and D) co-expression on TRESK (A and B) or TREK1 (C and D) currents in HEK 293T cells. Currents were elicited by voltage-ramps (from -100 to 100 mV, 1s duration). (E) Bar graph summarizing the relative TRESK, TREK1 and TREK2 current amplitudes at 0 mV when MT1 or MT2 are co-expressed. Student's *t* test (***) $P < 0.001$. (F) Representative images showing that GFP-MT2, but not GFP-MT1, can be pulled down by HA-TREK1 and HA-TREK2 via an anti-HA antibody in the SiMPull assay with HEK 293T cells.

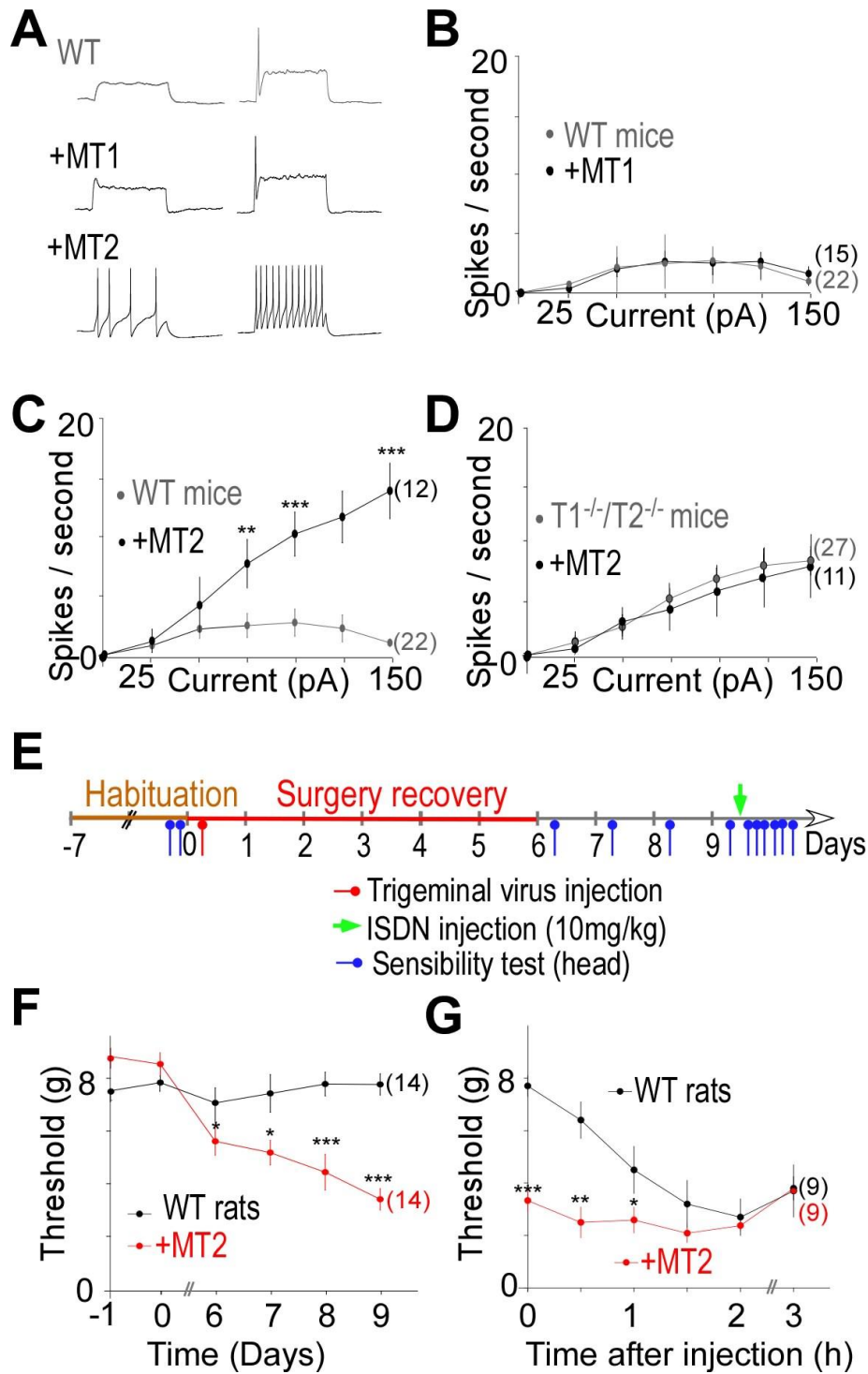


Figure 7. MT2, but not MT1, increases neuronal excitability of WT small TG neurons through TREK1 and TREK2 inhibition. (A) Representative traces showing spikes generated by incremental depolarizing current injections (+50 pA and +100 pA) in small-diameter TG neurons. (B and C) Input-output plots of spike frequency in response to 1s depolarizing current injection injections in WT small-

diameter TG neurons transfected with either GFP (“WT”), the GFP-tagged MT1 subunit (“MT1”) (**B**) or the GFP-tagged MT2 subunit (“MT2”) (**C**). (**D**) Input-output plots of spike frequency show a lack of effect of GFP-MT2 expression on TG neurons from TREK1/TREK2 double KO mice (T1^{-/-}/T2^{-/-}). (**E-G**) MT2 expression in TG leads to facial mechanical allodynia in rats. (**E**) Schematic of experimental behavioral paradigms. After a week of habituation rat were injected with 10 μl of AAV2 encoding for either MT2 + GFP or GFP. (**F**) Face withdrawal mechanical threshold assessed after trigeminal virus infection encoding either GFP (WT rat condition) or MT2. (**G**) Face withdrawal mechanical threshold, assessed after the first ISDN injection. The threshold for MT2 expressing rats were significantly decreased before the injection and remained less than WT for the first 1.5 hrs following ISDN injection. The numbers of tested cells and rats are indicated in parentheses. Student's *t* test (*P< 0.05, **P< 0.01, ***P< 0.001).

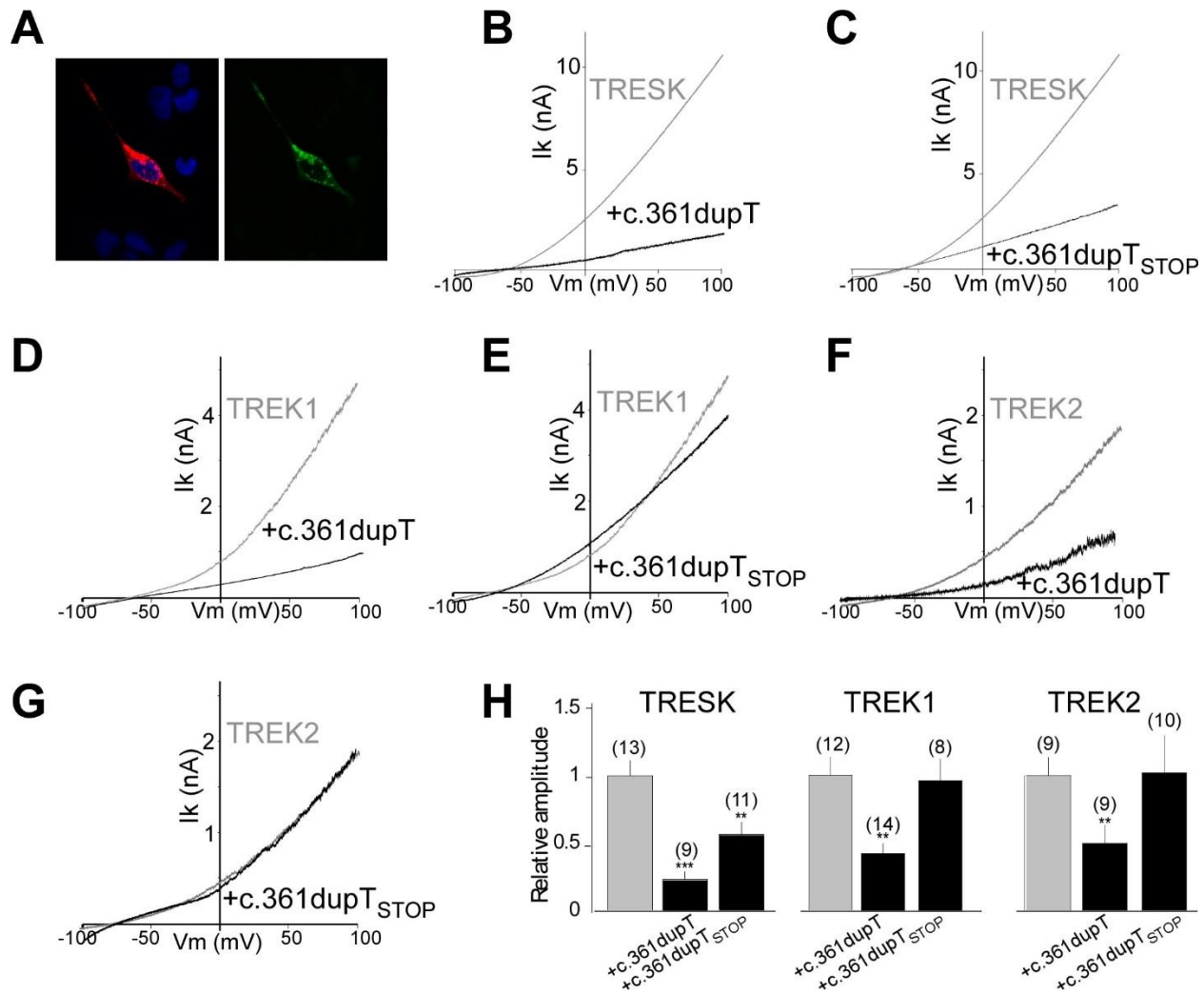


Figure 8. TRESK-c.361dupT (Y121LfsX44) acts as a dominant negative to reduce both TRESK and TREK1 current. (A) Co-synthesis of mCherry-MT1 and MT2-GFP products from the mCherry-TRESK-c.361dupT-GFP cDNA in HEK 293T cells. (B, C) Representative traces showing the effect of TRESK c.361dupT (B) and TRESK c.361dupT_{STOP} (C) co-expression on TRESK current. Currents were elicited by voltage-ramps (from -100 to 100 mV, 1s duration). (D, E) Same as (B, C) for TREK1. (F, G) same as (A, B) for TREK2. (H) Bar graph summarizing the relative TRESK, TREK1 and TREK2 current amplitudes at 0 mV for TRESK, TREK1 and TREK2 when TRESK c.361dupT and TRESK c.361dupT_{STOP} are coexpressed. Student's *t* test (***P*<0.01 and ****P*< 0.001).

Supplementary Materials for

Migraine-associated TRESK mutations increase neuronal excitability through alternative translation initiation and inhibition of TREK

Perrine Royal, Alba Andres-Bilbe, Pablo Ávalos Prado, Clément Verkest, Brigitte Wdziekonski, Sébastien Schaub, Anne Baron, Florian Lesage, Xavier Gasull, Joshua Levitz, Guillaume Sandoz*

Correspondence to: sandoz@unice.fr

This file includes:

Figs. S1 to S11

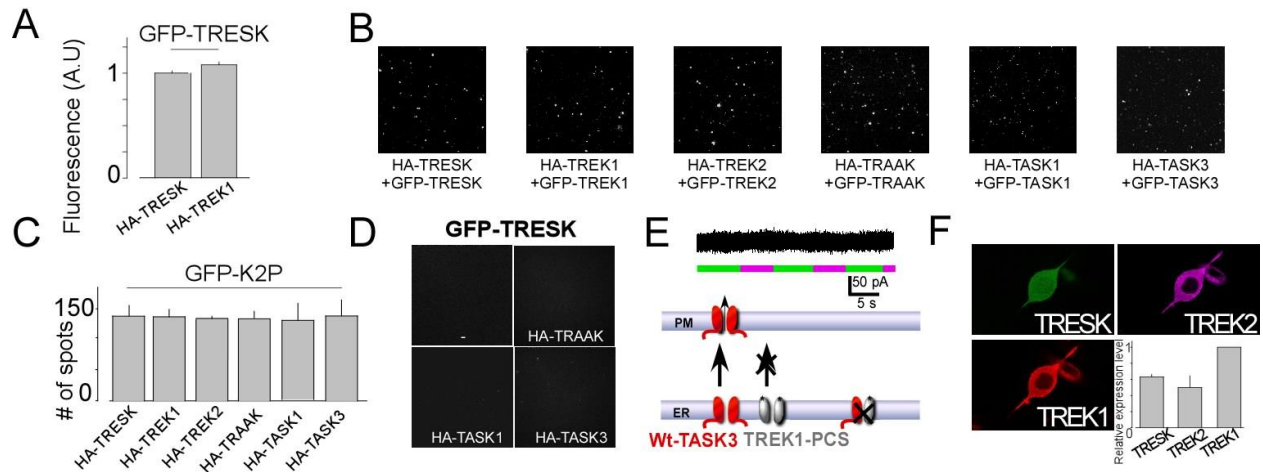


Figure S1. SiMPull assay controls. (A) GFP-fluorescence intensity of lysates from cells expressing HA-TRESK + GFP-TRESK or HA-TREK1 + GFP-TRESK. (B-C) Representative images and summary bar graph showing that HA-TREK1 pulldown GFP-TREK1, HA-TREK2 pulldown GFP-TREK2, HA-TRESK pulldown GFP-TRESK, HA-TRAAK pulldown GFP-TRAAK, HA-TASK1 pulldown GFP-TASK1 and HA-TASK3 pulldown GFP-TASK3. (D) Representative images showing that HA-TRAAK or HA-TASK1 or HA-TASK3 are not able to pull down GFP-TRESK and the control (-) showing that there are no fluorescent spots in the absence of antibody. (E) TREK1-PCS expression with TASK3 does not lead to photocurrent, indicating that TREK1 and TASK3 do not physically or functionally interact. (F) TREK1, TREK2 and TRESK are co-expressed in TG neurons. Immuno-detection of TREK1, TREK2 and TRESK. Inset, bar graph representing the average relative mRNA expression of TREK1, TREK2, TRESK obtained from 4 single cell semi-quantitative RT-PCR.

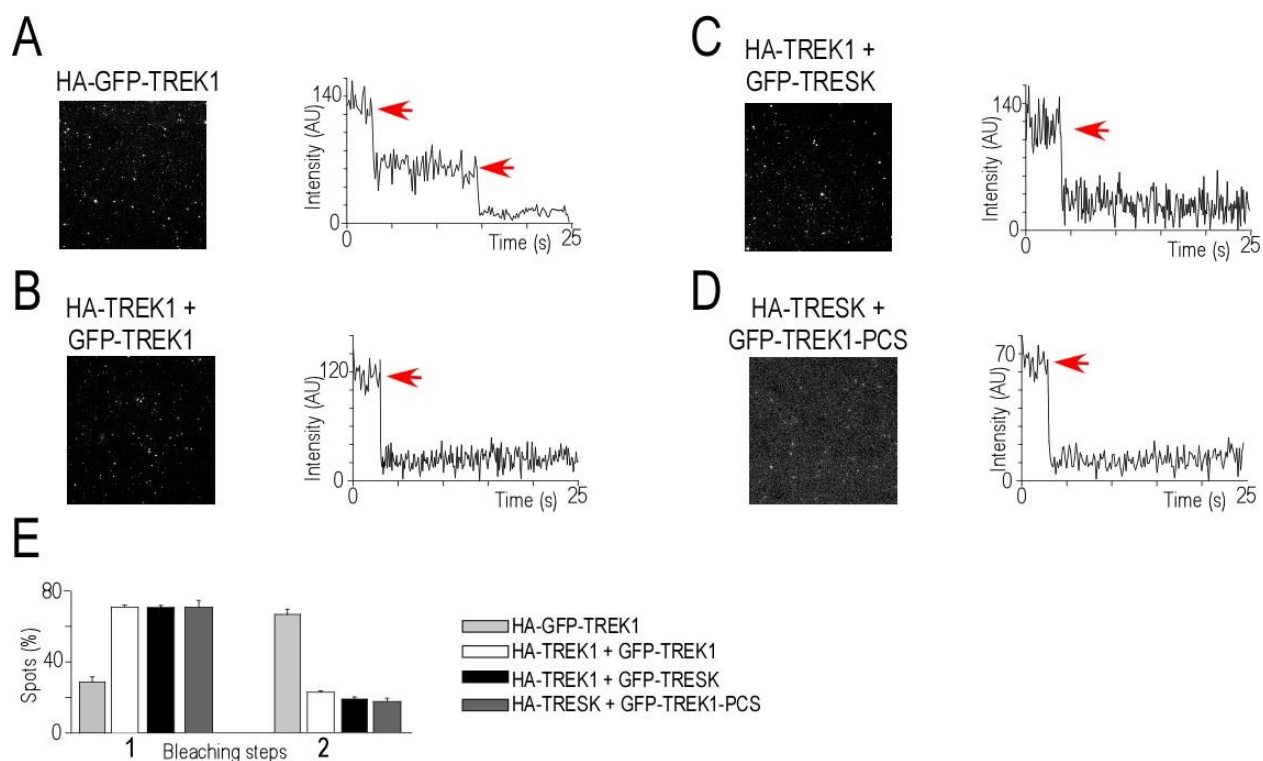


Figure S2: TRESK-TREK1 forms a dimer. (A) SiMPull assay for dimer control, left, TIRF images of HA-GFP-TREK1 single molecules, right, representative trace showing two-step photobleaching of HA-GFP-TREK1. (B) Same as in (A) for monomer control, HA-TREK1 pulldown of GFP-TREK1. (C) Same as in (A) for HA-TREK1 pulldown of GFP-TRESK. (D) Same as in (A) for HA-TRESK pulldown of GFP-TREK1-PCS. (E) Summary of photobleaching step distribution for HA-GFP-TREK1, HA-TREK1 pulldown of GFP-TREK1 and HA-TREK1 pulldown of GFP-TRESK and HA-TRESK pulldown of GFP-TREK1-PCS. AU, Arbitrary Unit.

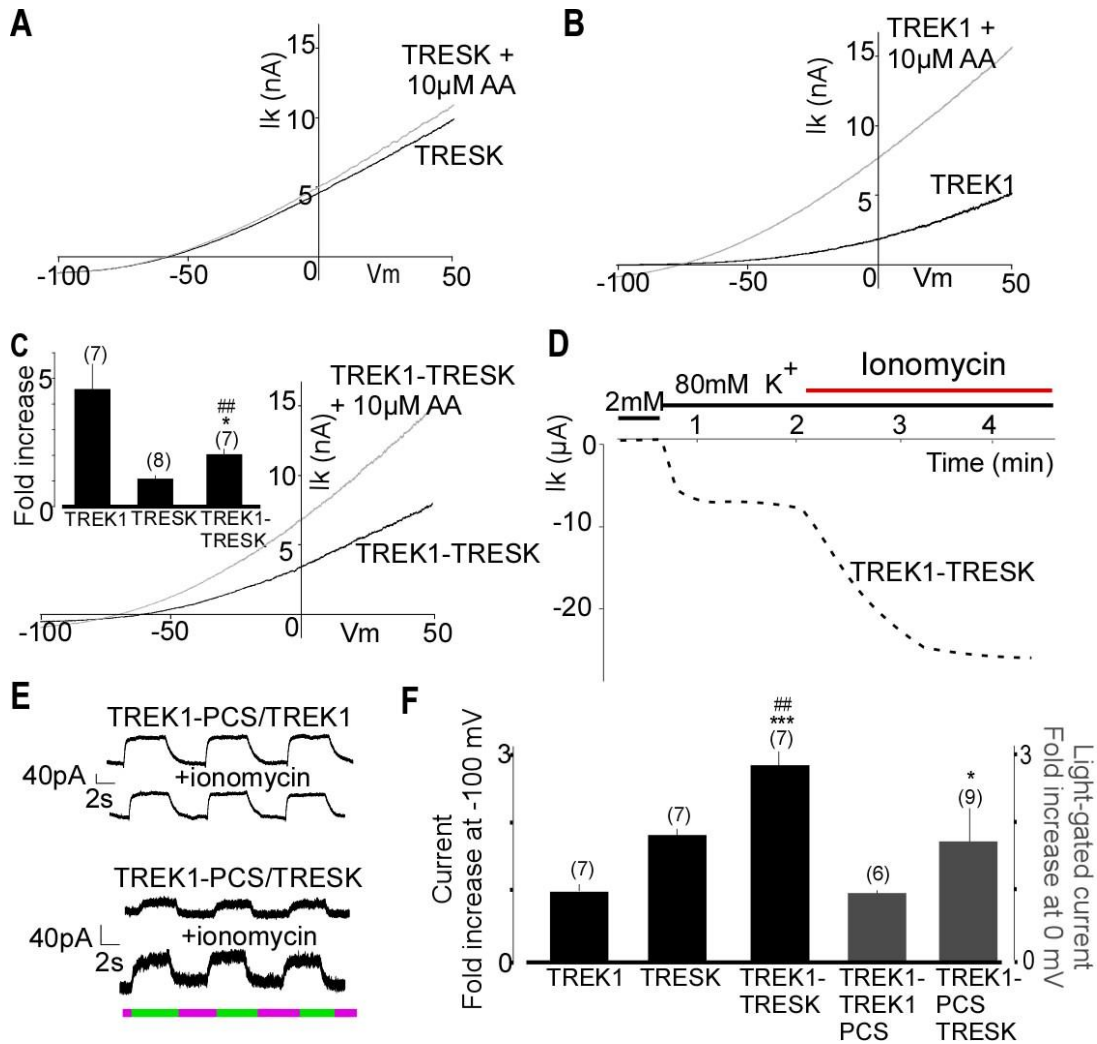


Figure S3. Functional characterization of TREK1-TRESK heterodimers. (A-C) Representative traces of TRESK (A) and TREK1 (B) and TREK1-TRESK (C) currents showing the effect of 10µM arachidonic acid application. Inset, summary of relative current amplitudes in HEK293T cells. (D) Representative TREK1-TRESK current amplitude modification induced by application of 0.5µM ionomycin, in *Xenopus* oocytes (E) Representative example of the effect of ionomycin on the light-gated currents of TREK1/TREK1PCS and TREK1-PCS/TRESK. Alternating illumination at 500 nm (green) and 380 nm (magenta) reversibly blocks and unblocks, respectively, the constant outward current, both with or without ionomycin, but the amplitude of the photomodulation for TRESK/TREK1PCS is bigger in the presence of ionomycin, in HEK293T cells.. (F) Summary of relative current amplitudes and their response to ionomycin.

Student's *t* test (**P* < 0.05, ***P* < 0.01, ****P* < 0.001 for TREK1-TRESK vs TREK1 and ##*P* < 0.01 for TREK1-TRESK vs TRESK).

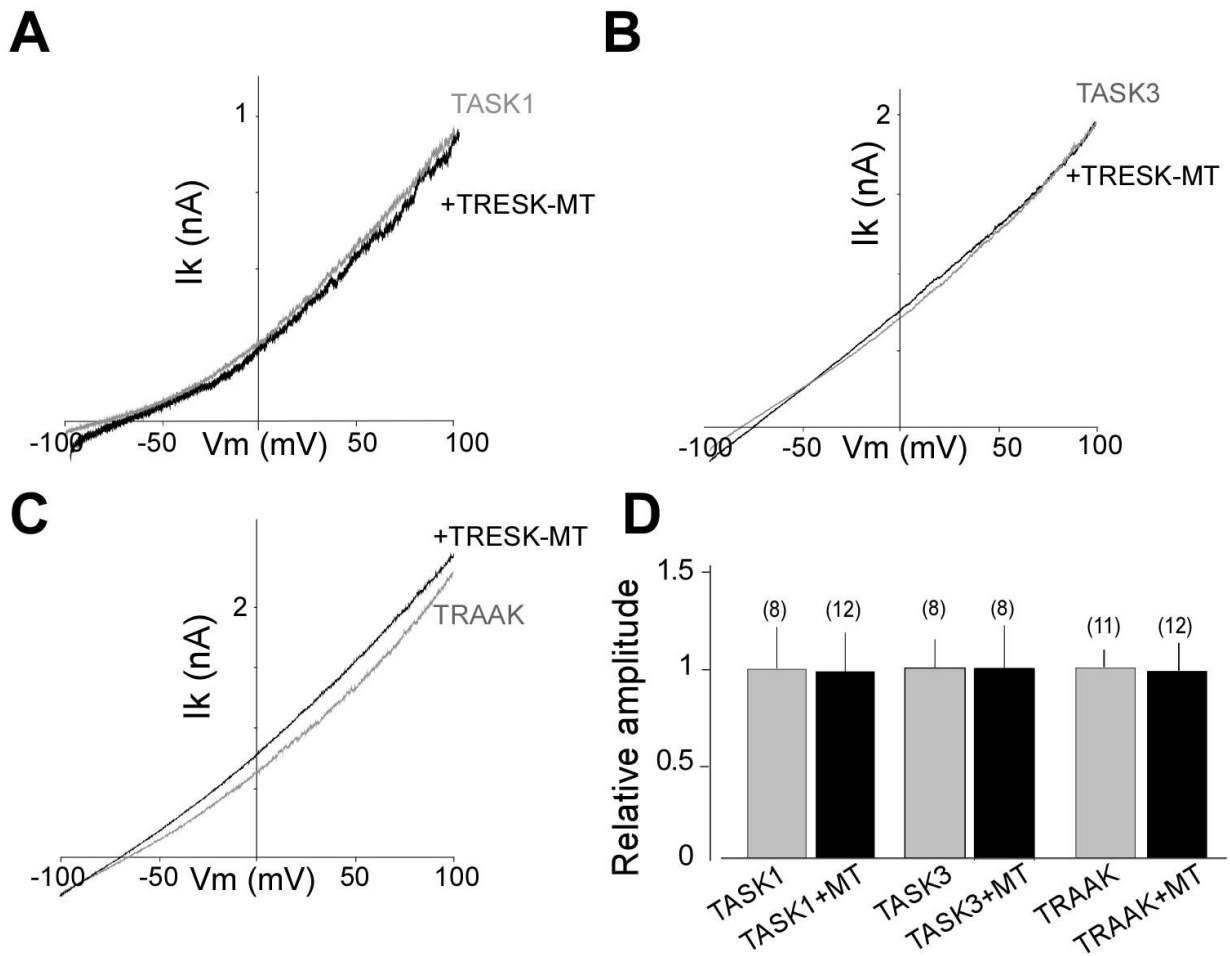


Figure S4. TRESK-MT does not inhibit TRAAK, TASK1 or TASK3. (A to C) Representative traces showing the effect of TRESK-MT co-expression TASK1 (A), TASK3 (B) or TRAAK (C) currents. Currents were elicited by voltage-ramps (from -100 to 100 mV, 1s duration). (D) Bar graph summarizing the relative TASK1, TASK3, or TRAAK current amplitudes at 0 mV with or without TRESK-MT co-expression.

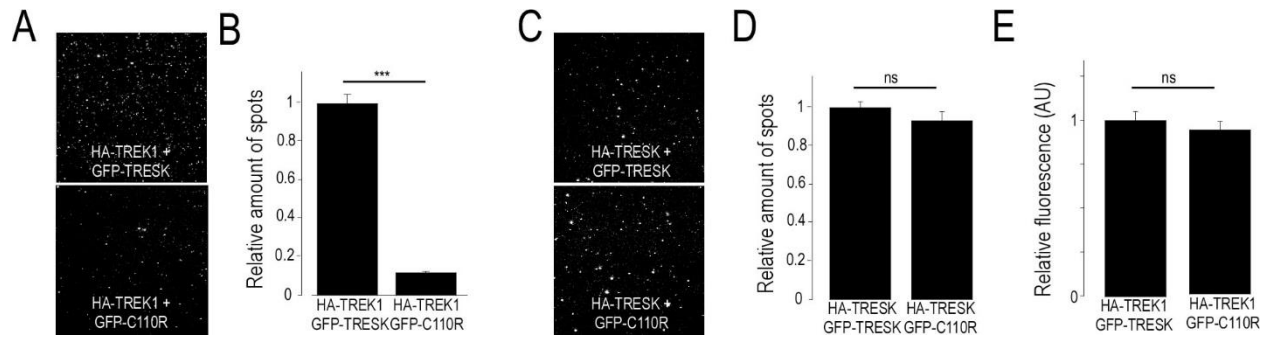


Figure S5. TRESK-C110R mutation inhibits TRESK-TREK1 association. Representative images showing HA-TREK1 pull down of GFP-TRESK and GFP-TRESK-C110R via an anti-HA antibody. **(B)** Bar graph showing the relative pulldown of GFP-TRESK and GFP-TRESK-C110R by HA-TREK1. Both conditions were done on the same day at the same dilution. **(C and D)** Same as (A and B) for HA-TRESK pull down of GFP-TRESK and GFP-TRESK-C110R. Student's *t* test (***) $P < 0.001$. **(E)** GFP-fluorescence intensity of lysate from HA-TREK1 + GFP-TRESK and HA-TREK1 + GFP-TRESK-C110R cells showing that GFP-TRESK and GFP-TRESK-C110R are expressed at similar levels in HEK 293T cells.

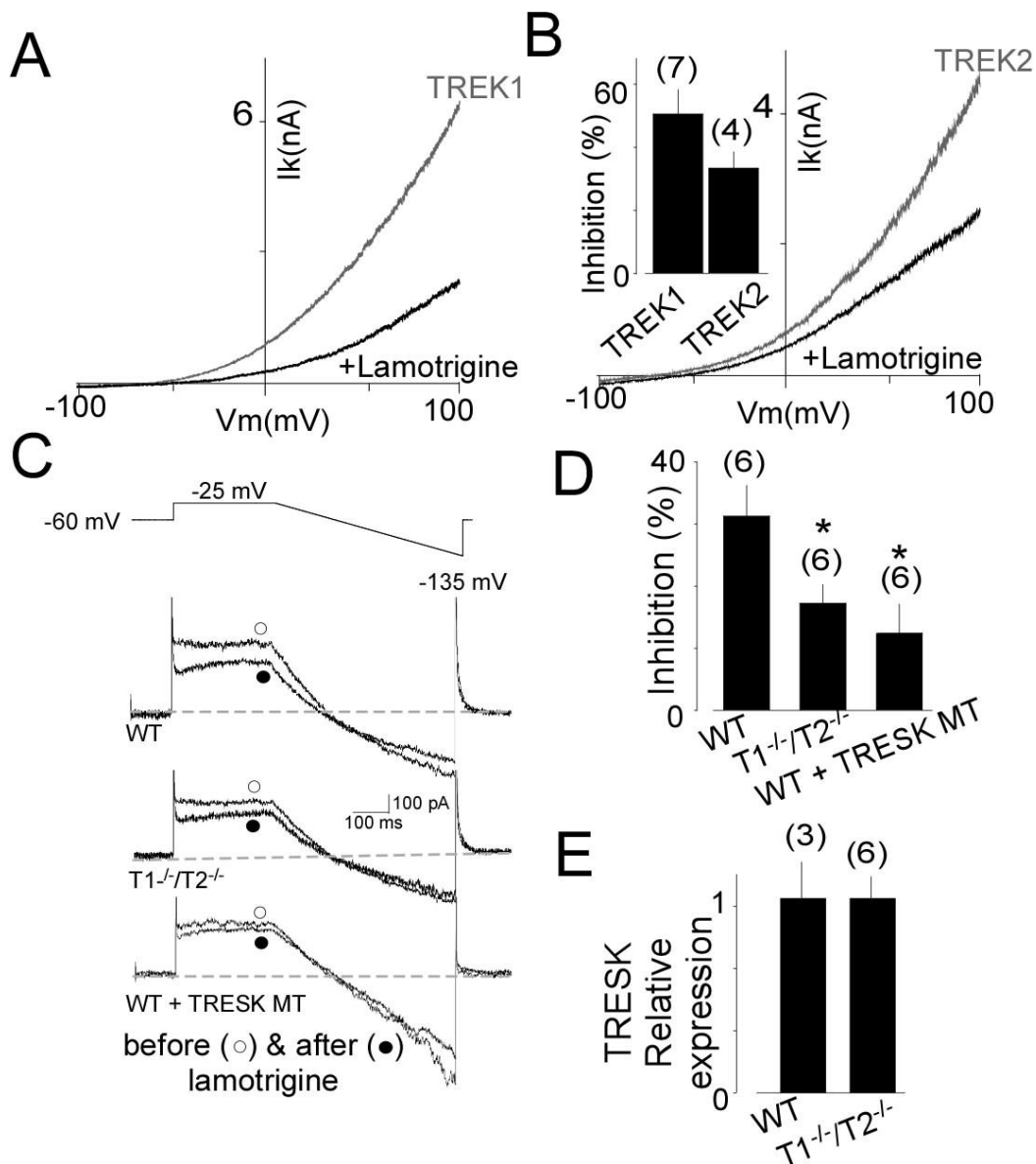


Figure S6. The lamotrigine sensitive leak current is reduced in TG neuron from TREK1^{-/-}/TREK2^{-/-} KO mice. (A) Representative traces of TREK1 (A) and TREK2 (B) showing the effect of 30 μ M lamotrigine application in HEK293T cells. Inset, summary of inhibition induced by lamotrigine application. (C) Representative current traces from WT TG neurons expressing GFP (WT) or TRESK-MT (WT + TRESK-MT) and from TREK1^{-/-}/TREK2^{-/-} (T1^{-/-}/T2^{-/-}) TG neuron expressing GFP (T1^{-/-}/T2^{-/-}). (D) Percentage of outward current (measured at the end of the depolarizing step) inhibited by lamotrigine. (E) Relative expression of TRESK in WT and T1^{-/-}/T2^{-/-} mice.

Relative TRESK expression. TREK1 and 2 invalidation did not change the expression of TRESK. The numbers of tested cells or tissues are indicated in parentheses.

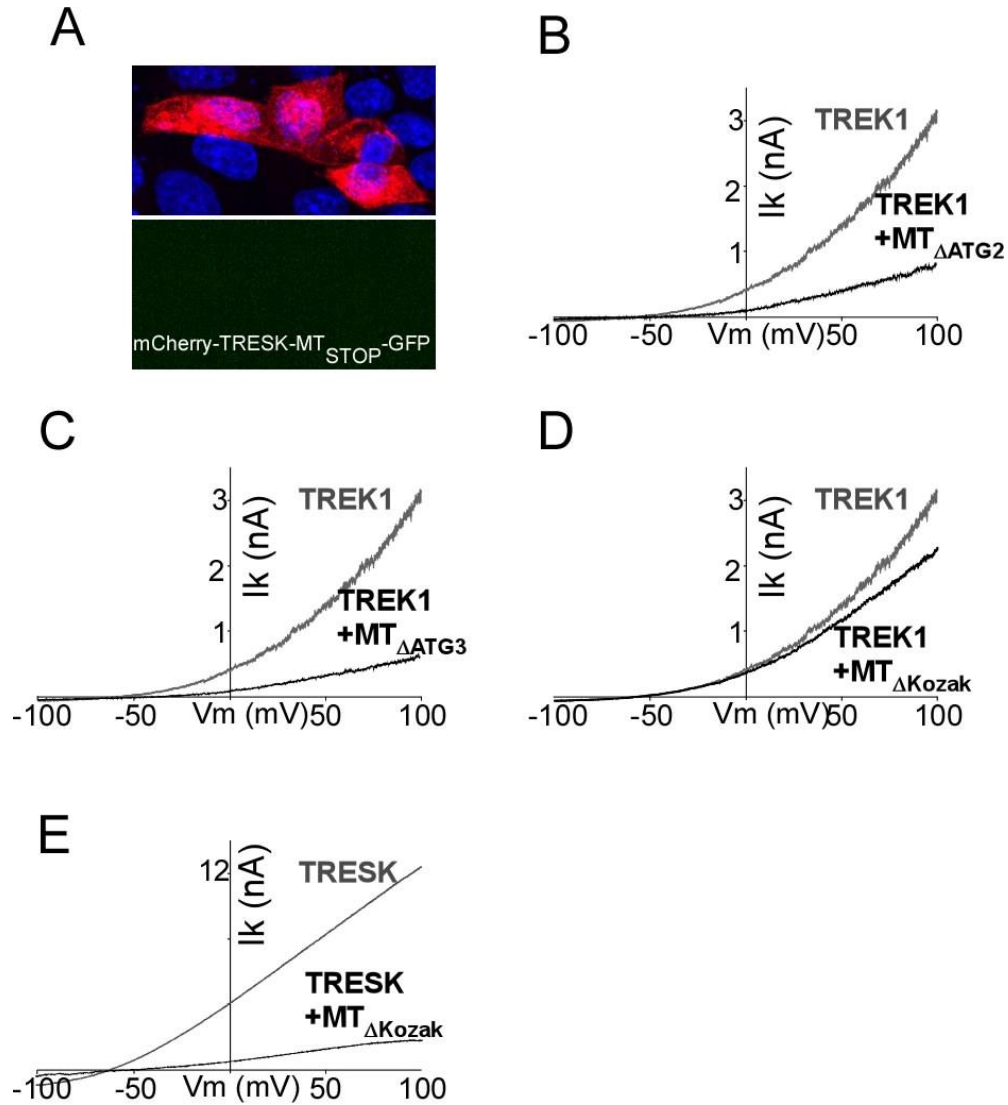


Figure S7. MT2 is cotranslated with MT1 and mediates TREK1 inhibition. (A) Introduction of a stop codon into the MT2 ORF of mCherry-TRESK-MT-GFP (mCherry-TRESK-MT_{STOP}-GFP) induces a loss of the GFP fluorescence in HEK 293T cells (B-D) Representative traces showing the effect of introduction of a mutation of ATG2 (MT_{ΔATG2}) (B), ATG3 (MT_{ΔATG3}) (C) and ΔKozak (MT_{ΔKozak}) (D) on TRESK-MT on TREK1 current in HEK 293 T cells. (E) Representative traces showing the effect of TRESK-MT_{ΔKozak} on TRESK current.

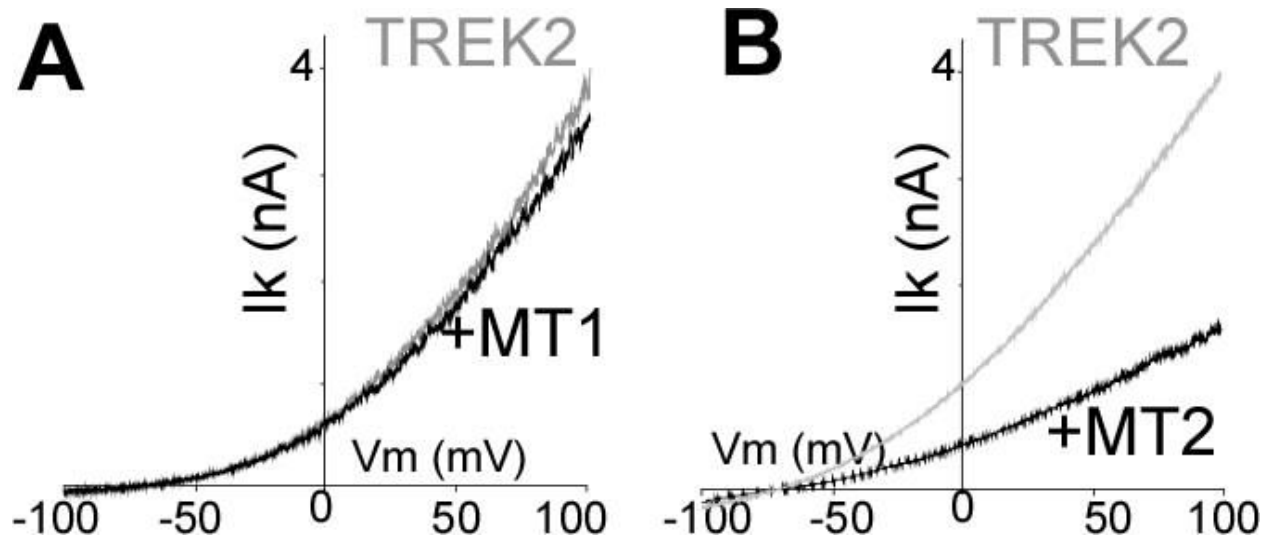


Figure S8. MT2, but not MT1, acts as a dominant negative on TREK2 channels. (A and B) Representative traces showing the effect of TRESK-MT1 (A) or TRESK-MT2 (B) co-expression on TREK2 current.

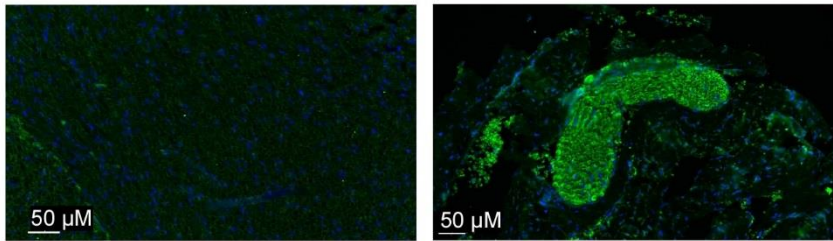
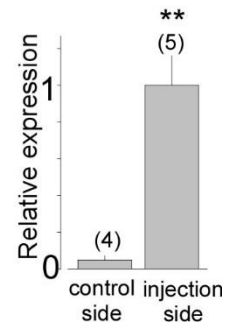
A**B**

Figure S9. Viral expression of TRESK-MT2 pIRES 2 EGFP into trigeminal neurons. (A) The viral expression into trigeminal ganglia marked by the coexpressed-EGFP protein labelled in green (right). (B) Quantification of the viral infection through quantitative PCR 9 days post injection.

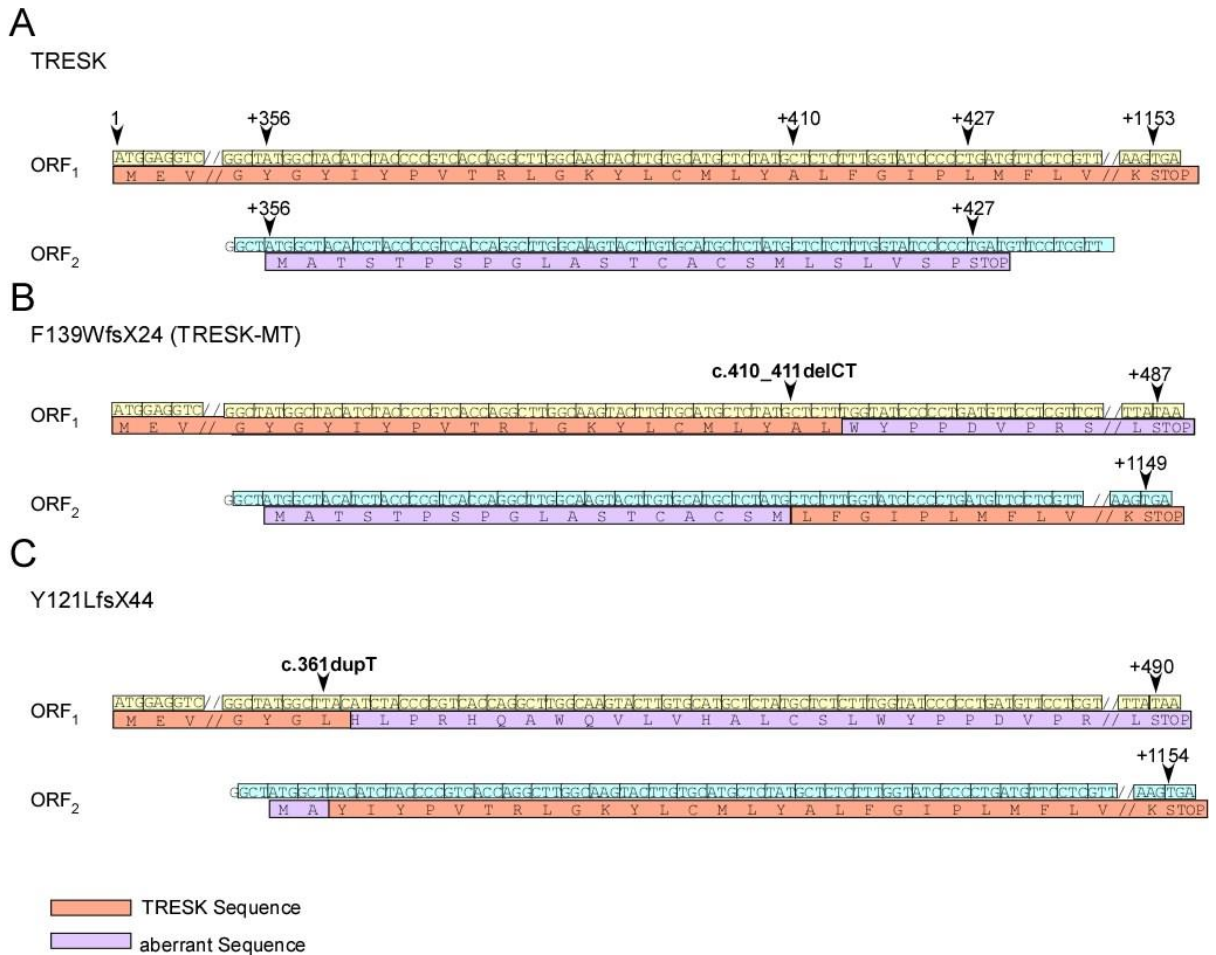


Figure S10. Sequence organization of TRESK, TRESK-F139WfsX24 and TRESK-Y121LfsX44. (A) cDNA sequence of TRESK and deduced amino acid sequence for ORF1 and ORF2, (B) 2 pb deletion c.410_411delCT resulting in the change of reading frame leading to a premature stop codon in ORF1 at position +427 (MT1) and putting the ATG +356 in frame with the reference open reading frame of TRESK inducing the production of MT2. (C) 1 pb insertion c.361dupT resulting, as c.410_411delCT, in the change of reading frame leading to a premature stop codon in ORF1 at position +490 (MT1) and putting the ATG +356 in frame with the reference open reading frame of TRESK inducing the production of MT2.

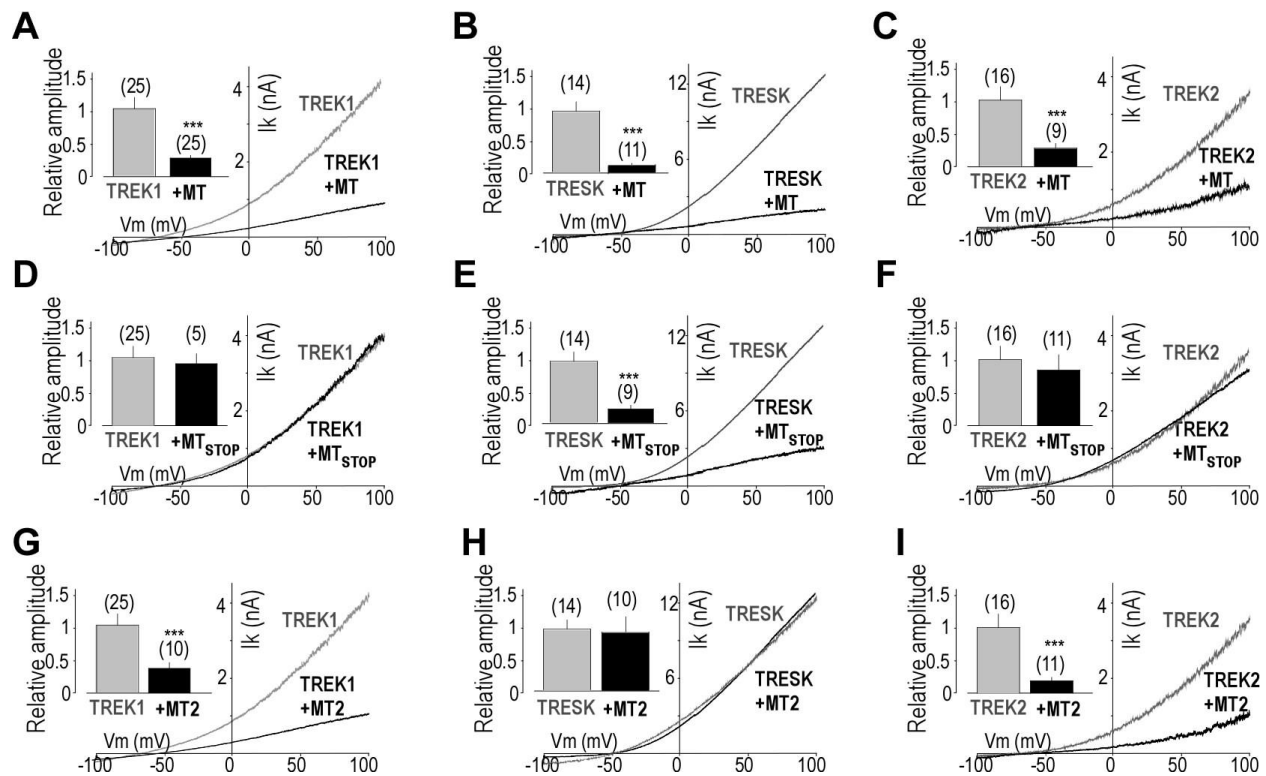


Figure S11. Regulation of the hTRESK, hTREK1 and hTREK2 by hTRESK-MT, hTRESK-MT_{STOP} and hMT2. (A-C) Representative traces and insets showing the effect of co-expression of hTRESK-MT on hTREK1 (A) hTRESK (B) and hTREK2 (C) currents HEK 293T cells. (D-F) Representative traces and insets showing the effect of hTRESK-MT_{STOP} on hTREK1 (D), hTRESK (E), and hTREK2 (F) currents. (G-I) Representative traces and insets showing the effect of hTRESK-MT2 co-expression on hTREK1 (G), hTRESK (H), and hTREK2 (I) currents in HEK293T cells. Currents were elicited by voltage-ramps (from -100 to 100 mV, 1s duration). The numbers of cells tested are indicated in parentheses. Student's *t* test (**P*< 0.05, ***P*< 0.01, ****P*< 0.001) shows the difference between hTREK1 or hTRESK or hTREK2 and hTREK1 or TRESK or TREK2 when co-expressed with different TRESK-MT constructs.